A CONTROL ALLOCATION TECHNIQUE TO RECOVER FROM DRIVER-INDUCED OSCILLATIONS

A THESIS SUBMITTED TO

THE GRADUATE SCHOOL OF ENGINEERING AND SCIENCE

OF BILKENT UNIVERSITY

IN PARTIAL FULFILLMENT OF THE REQUIREMENTS FOR

THE DEGREE OF

MASTER OF SCIENCE

IN

MECHANICAL ENGINEERING

By

Ayesha Sarwar

December 2019

A control allocation technique to recover from driver-induced oscillations

By Ayesha Sarwar

December 2019

We certify that we have read this thesis and that in our opinion it is fully adequate, in scope and in quality, as a thesis for the degree of Master of Science.

Yildiray Yildiz(Advisor)

Onur Özcan

Mustafa Mert Ankaralı

Approved for the Graduate School of Engineering and Science:

Ezhan Karaşan
Director of the Graduate School

ABSTRACT

A CONTROL ALLOCATION TECHNIQUE TO RECOVER FROM DRIVER-INDUCED OSCILLATIONS

Ayesha Sarwar
M.S. in Mechanical Engineering
Advisor: Yildiray Yildiz
December 2019

The focus of this thesis is the study of driver induced oscillations. When the rear tires of a car are force saturated due to aggressive driver behaviour, high velocity on a slippery road, sudden steering action or heavy braking, rear end of the car tends to lose traction on the road and starts skidding. At the same time, the driver, having the direct steering control over the front two tires, feels a time delay at the response of the rear tires to the steering actions. The delay between the driver's action and the vehicle's response may eventually instigate the swinging of the rear end of the vehicle, which is generally referred to as "fishtailing". In the literature, few studies exist regarding fishtailing motion and in those studies, the theoretical background of this motion is not studied in detail. In this thesis, fishtailing motion dynamics are investigated in detail by employing a non linear vehicle model, and this motion is recreated for a specific vehicle configuration. Then, a control allocation technique is presented to recover from this driver-induced fishtailing motion. The proposed control allocation method helps the vehicle recover from these undesired oscillations by minimizing the phase shift between the commanded and realized forces and moments. The simulation results demonstrate that using the proposed method, it is possible to make the vehicle recover from driver induced oscillations even at high velocities where conventional approaches fail. For the cases of actuator failure, for example loss of tire inflation pressure, an adaptive version of the control allocation is also proposed that can stabilize the vehicle even when the actuator effectiveness is reduced significantly.

Keywords: Automotive Control, Control allocation.

ÖZET

SÜRÜCÜ KAYNAKI SALINIMLARI SÖNÜMLEMEK İÇİN KONTROL DEĞİTİM METODU GELİŞTİRİLMESİ

Ayesha Sarwar
Makine Mühendisliği, Yüksek Lisans
Tez Danışmanı: Yildiray Yildiz
Aralık 2019

Bu tezin odak noktası, sürücü kaynaklı salınımların incelenmesidir. Bir otomobilin arka lastikleri üzerindeki kuvvetler, agresif sürücü davranışları, kaygan yolda yapılan yüksek hızlar, ani direksiyon hareketleri veya ani frenler nedeniyle doygunluğa ulaştığında, aracın arka kısmı yola tutunamaz ve kaymaya başlar. Kaymayla birlikte, sürücü aracın direksiyon hareketlerine geç cevap verdiğini farketmeye başlar. Sürücü girdileriyle aracın cevapları arasında oluşan bu zaman gecikmesi aracın arka kısmının salınım yapmaya ya da bir diğer adıyla savrulmaya başlamasına sebep olabilir. Literatürde savrulma dinamikleri pek az incelenmiştir ve yapılan incelemelerde verilen detaylar da teorik bir inceleme için yeterli değildir. Bu çalışmada savrulma hareketi doğrusal olmayan araç modelleri ışığı altında incelenmiş ve bu hareket belirli bir araç konfigürasyonunda simülasyon ortamında yeniden üretilmiştir. Daha sonra savrulma hareketinden aracı çıkarmak için bir kontrol dağıtım metodu önerilmiştir. Bu kontrol dağıtım metodu, sürücünün araçtan talep ettiği kuvvet ve momentler ile gerçekleştirilen kuvvet ve momentler arasındaki faz farkını minimize ederek salınımların sönümlenmesini sağlamaktadır. Önerilen metodun, alternatif metotların zorlandığı yüksek hızda oluşan salınımları sönümleme işinde başarılı olduğu simülasyonlar aracılığı ile gösterilmiştir. Ayrıca, önerilen metodun uyarlamalı bir versiyonu, eyleyicilerin etkilerinin bir kısmını kaybettikleri durumlar için geliştirilmiştir. Uyarlamalı kontrol dağıtıcısının önemli eyleyici etkinlik kayıplarında aracın kararlılığını sağladığı da gösterilmiştir.

Anahtar sözcükler: Otomotiv Kontrolü, Kontrol tahsisi.

Acknowledgement

I acknowledge that ...

Contents

List of Figures

List of Tables

Chapter 1

Introduction

1.1 Driver Induced Oscillations

A pilot induced oscillation (PIO) can be defined as an undesired, persistent oscillation of the aircraft, due to an abnormal coupling between the pilot and the aircraft [1, 2]. A similar phenomenon can be observed in driver-vehicle interactions, causing the vehicle body swing dangerously, which can be named as driver induced oscillations (DIO) [3]. The focus of this thesis is a specific kind of DIO, which is called "fishtailing". Fishtailing is an uncontrolled over-steer event, where the rear wheels lose traction on the road. During fishtailing, the rear tires reach their side force saturation limit, lose their grip on the road and start slipping sideways [4]. The saturation of the tire lateral forces manifests itself as a delay in the vehicle's response to driver steering inputs. While the driver makes an effort to control the vehicle by steering it in the opposite direction to offset the side slip, the delayed vehicle response may cause an overreaction by the driver and make the rear end of the car slip in the opposite direction. This rear end oscillation gives the incident its name: fishtailing. A representation of the fishtailing event is depicted in Fig. 1.1, where the car on the left experiences fishtailing. The car on the right, following a straight path, is shown to create contrast.

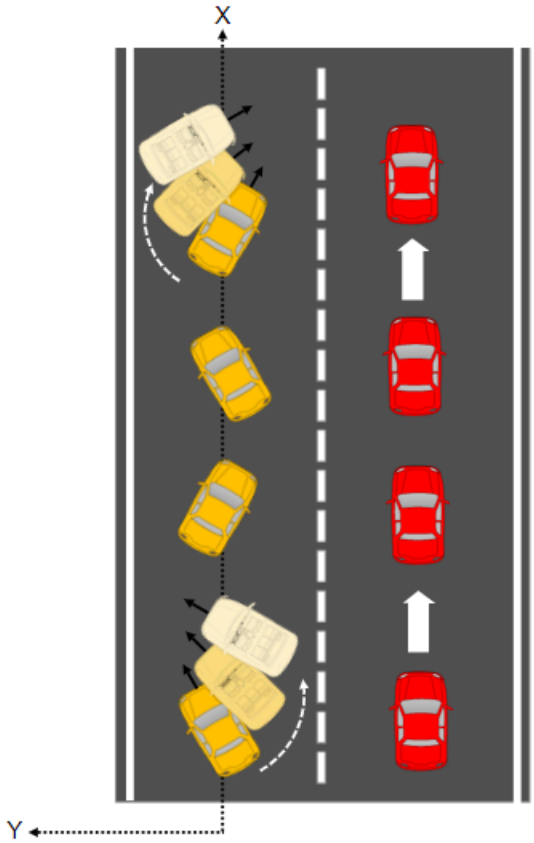

Figure 1.1: Fishtailing behaviour of car.

1.2 Related Work

There are several driver assistance systems which are already integrated in modern cars to increase vehicle stability. Traction control system (TCS), for example, is used to prevent wheel slippage via modulating both the traction forces (through engine control) and braking forces [5]. While very useful, TCS only helps with limiting the wheel slippage but does not help directly with directional control in extreme situations of under-steer and over-steer. Electronic stability program (ESP), on the other hand, assists the driver in under-steer and over-steer situations to maintain the driver's intended path trajectory, by controlling the traction and braking forces of one or more wheels simultaneously. For example, during

under-steer, ESP applies brakes on inner wheels and releases on outer wheels slightly to reduce the turning radius to keep the vehicle on driver's intended path. In both TCS and ESP, braking interventions can have significant effect on forward speed. Active steering system, another technology currently in use, is employed for recovering lateral stability without the loss of longitudinal speed, by superimposing steering corrections, in the presence of sudden or unexpected yaw disturbances. It is capable of adjusting steering ratio at low or high speeds by altering the relation between driver steering wheel angle and tire wheel angle [6].

In the past few years, many novel ideas for chassis control are proposed that employ traction, braking and steering control tools. In [7], a yaw stability control design is proposed for electric vehicles equipped with steer-by-wire (SBW) system, using active front steering control. Another control approach is presented in [8] based on tracking a reference model's lateral, longitudinal and yaw moment dynamics by utilizing four wheel SBW. In [9], an assistance control for lane-keeping is presented using brakes as actuators. [10] conducted a study on control of torque-vectoring differentials to reduce side slip angle during a double lane changing maneuver. In [11], using differential braking as an actuator, a control allocation algorithm for yaw stabilization and roll-over prevention based on side slip angle minimization is developed. A control approach is presented in [12] for unknown road conditions to minimize tire slip angle using four wheel independent braking actuators.

Combining individual traction, braking and steering control tools, and thus forming an "integrated chassis controller", has also proved to be an effective vehicle control strategy. An integrated chassis control approach for path tracking is presented by [13] using driving forces and steering angles as control inputs. Controllers for lateral stability are presented by [14] and [15], which combine active front steering (AFS) and direct yaw moment control (DYC). A model predictive control based strategy, combining AFS and differential braking, is proposed by [16] for yaw stability. [17] and [18], introduce coordinated control strategies that utilize traction and braking torques. A control framework for lateral stabilization is presented by [19], which integrates differential braking and traction

torque transfer. [20] proposes an integrated envelope control method for path tracking of an autonomous 4-wheel drive vehicle. An active steering and adaptive brake control allocation approach is presented for vehicle yaw stabilization in [21]. Similarly, several other studies on integrated vehicle control are conducted, which make use of commercially available conventional control systems [22, 23, 24, 25, 26].

One of the effective technologies exploited in the studies discussed above is *control allocation (CA)*. A control allocator distributes the control input generated by the controller to redundant actuators. In automotive control applications, the control input generally consists of forces and moments to be applied on the vehicle [11, 18, 19, 22, 27].

1.3 Contribution of This Study

In this study, we propose a CA structure specifically designed to address the fishtailing motion. To the best of authors' knowledge, no prior work exist in the open literature that study the fishtailing motion in the automotive integrated chassis control context. Already available conventional control systems such as ESP and TCS can help minimize under/over-steer but the utilization of these technologies for the elimination of, or the recovery from, the fishtailing event is not discussed rigorously in the literature. The main idea of the proposed CA, inspired from [28] and [29], emerges from the observation that the desired and achieved forces and moments are out of phase during fishtailing. Fig. 1.2 shows the desired/reference and achieved/actual yaw moments during a fishtailing event, which will be discussed in more detail later in this study. It is seen that the phase shift creates an effective time delay in the system, which is known for its destabilizing effect in control systems. Combined with the compensating maneuvers of the driver, this effective time delay causes sustained vehicle oscillations. The proposed method synchronizes the out-of-phase signals and thus helps the vehicle recover from fishtailing. This is achieved by using optimal control allocation to minimize a carefully constructed cost function that penalizes the derivative error

between the desired and achieved signals. Once this error is minimized, the phase shift is eliminated and the oscillations are damped out.

It is demonstrated through simulation studies that the proposed control structure is capable of eliminating the oscillatory motion of the vehicle at high velocities where conventional control allocations fail.

Another contribution of this study is that an adaptive control allocation approach is proposed for a more challenging scenario where the vehicle is stuck in a driver induced oscillation in the presence of actuator failure such as a flat tire. The proposed control allocation approach to recover from driver induced oscillations discussed above is not adaptive and may not be able to stabilize the vehicle in the extreme case of actuator failures. Hence, an adaptive version of this control allocator, inspired by [30], is developed. Adaptive CA approach minimizes the derivative error between the virtual and actual control efforts while tolerating the actuator uncertainty.

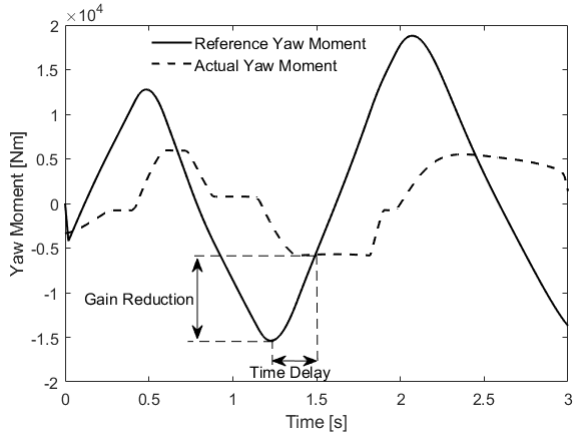

Figure 1.2: Phase shift between the desired/reference and achieved/actual yaw moments.

Chapter 2

Reproducing a Specific Kind of Driver Induced Oscillation: Fishtailing

In vehicle dynamics control, lateral dynamics of a vehicle are of great importance. High percentage of road accidents occur during cornering, lane departure or lane changing maneuvers. Controlling lateral dynamics is challenging due to the possibility of the saturation of lateral tire forces and limited tire grip especially at high velocities on low friction roads. Lateral tire force saturation can lead to oversteer or understeer. Fishtailing is an uncontrolled oversteer event which makes the vehicle stuck in persistent oscillations by driver's aggressive input commands usually on a snowy road, leading to rear end of the car swinging behind the front end. In this chapter, the creation of a fishtailing event for a specific vehicle configuration is discussed. Furthermore, following questions are investigated related to the fishtailing motion:

- How is the tire slip angle generated?
- How do the rear tires develop larger tire slip angles compared to the front tires?
- Why are the rear tires prone to hitting the saturation limit faster than the front tires?

Table 2.1: Vehicle variables for 2-track model

δ_1	Front wheel steering angle[rad]
V	Longitudinal velocity at vehicle CG[m/s]
β	Side slip angle at vehicle CG[rad]
r	Yaw rate at vehicle CG[rad/s]
Y	Lateral displacement of vehicle CG from centre-line of lane [m]
Y_f	Vehicle front end lateral displacement from centre-line of lane [m]
m	Mass of vehicle[kg]
F_{Zi}	Normal load on i^{th} tire[N]
J_z	Moment of inertia along z-axis[kgm^2]
ψ	Yaw angle at vehicle CG[rad]
f_x	Total longitudinal force[N]
f_y	Total lateral force[N]
M	Yaw moment along z-axis at vehicle CG[Nm]
F_{Xi}	Longitudinal traction force (along tire X-axis) of i^{th} tire[N], where $i \in [1, 2, 3, 4]$
F_{Yi}	Lateral tire force (along tire Y-axis) of i^{th} tire[N]
$F_{x,fl}$	Longitudinal traction force (along vehicle x-axis) of front left tire[N]
$F_{x,fr}$	Longitudinal traction force (along vehicle x-axis) of front right tire[N]
$F_{x,rl}$	Longitudinal traction force (along vehicle x-axis) of rear left tire[N]
$F_{x,rr}$	Longitudinal traction force (along vehicle x-axis) of rear right tire[N]
L_f	Distance of front axle from vehicle CG[m]
L_r	Distance of rear axle from vehicle CG[m]
d	Width of wheelbase[m]
C_α	Cornering stiffness coefficient[1/rad]
α_i	Tire slip angle of i^{th} tire[rad], where $i \in [1, 2, 3, 4]$

2.1 Vehicle Modelling

In this section, the high-fidelity nonlinear 2-track vehicle model [5] is briefly explained . The introduction of the nonlinear model in this section sets the basis for the development of the specific state space representation required for control allocation implementation.

The geometry used for deriving the model is presented in Fig. 2.1 [27]. In this figure, the net forces acting on the center of gravity (CG) are given as $f_x \in \Re$ and $f_y \in \Re$. These forces can be calculated as

$$f_x = F_{x,fl} + F_{x,fr} + F_{x,rl} + F_{x,rr} \tag{2.1}$$

and

$$f_y = F_{y,fl} + F_{y,fr} + F_{y,rl} + F_{y,rr}, \tag{2.2}$$

where

$$F_{x,fl} = F_{X1}cos\delta_1 - F_{Y1}sin\delta_1, \tag{2.3}$$
$$F_{x,fr} = F_{X2}cos\delta_1 - F_{Y2}sin\delta_1, \tag{2.4}$$
$$F_{x,rl} = F_{X3}cos\delta_2 - F_{Y3}sin\delta_2, \tag{2.5}$$
$$F_{x,rr} = F_{X4}cos\delta_2 - F_{Y4}sin\delta_2, \tag{2.6}$$
$$F_{y,fl} = F_{Y1}cos\delta_1 + F_{X1}sin\delta_1, \tag{2.7}$$
$$F_{y,fr} = F_{Y2}cos\delta_1 + F_{X2}sin\delta_1, \tag{2.8}$$
$$F_{y,rl} = F_{Y3}cos\delta_2 + F_{X3}sin\delta_2, \tag{2.9}$$

and

$$F_{y,rr} = F_{Y4}cos\delta_2 + F_{X4}sin\delta_2. \tag{2.10}$$

It is noted that $\delta_i \in \Re, i = 1, 2$, in (2.3)-(2.10) are the steering angles shown in Fig. 2.1, and the subscripts "fl", "fr", "rl" and "rr" refers to front left, front right, rear left and rear right, respectively.

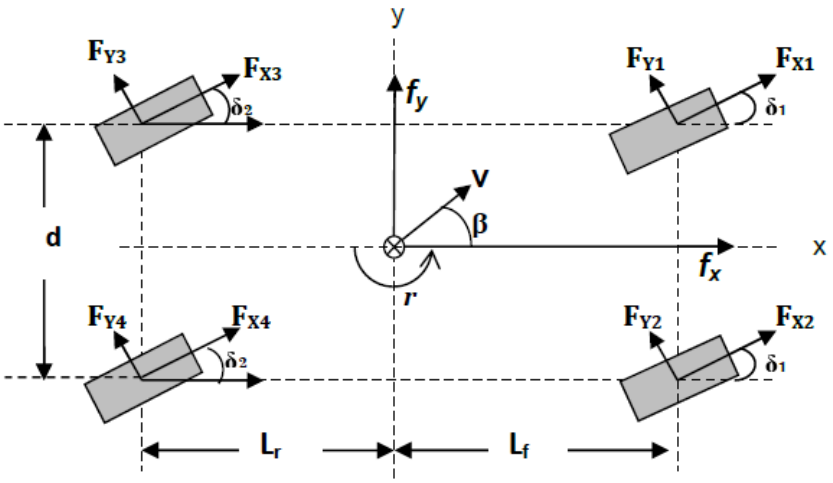

Figure 2.1: 2-track vehicle model.

The equations of motion, for a vehicle mass of m, in the direction of the velocity vector, V, and in the direction that is perpendicular to V are given as

$$m\dot{V} = f_x cos(\beta) + f_y sin(\beta) \tag{2.11}$$

and

$$mV(\dot{\beta} + r) = f_y cos(\beta) - f_x sin(\beta), \tag{2.12}$$

respectively. $\beta \in \Re$ represents the side slip angle and $r \in \Re$ is the yaw rate. Furthermore, the rotational dynamics is given as

$$M = J_z \dot{r}, \tag{2.13}$$

where $M \in \Re$ is the net moment about the yaw axis and $J_z \in \Re$ is the mass moment of inertia of the vehicle. M can be calculated as:

$$\begin{aligned} M =& (F_{x,fr} + F_{x,rr} - F_{x,fl} - F_{x,rl})d/2 + (F_{y,fl} + F_{y,fr})L_f - \\ & (F_{y,rl} + F_{y,rr})L_r, \end{aligned} \tag{2.14}$$

where the geometric parameters $L_f \in \Re$, $L_r \in \Re$ and $d \in \Re$ can be observed in Fig. 2.1.

In (2.3)-(2.10), the longitudinal tire forces, $F_{Xi} \in \Re$, $i = 1, 2, 3, 4$, are the traction forces generated by the controller. Lateral forces, $F_{Yi} \in \Re$, $i = 1, 2, 3, 4$,

are calculated as

$$F_{Yi} = C_\alpha \alpha_i F_{Zi}, \tag{2.15}$$

where $C_\alpha \in \Re$ is the lateral cornering stiffness coefficient, $F_{Zi} \in \Re$ is the normal force on tire i, and $\alpha_i \in \Re$ is the tire slip angle. Normal forces and tire slip angles are calculated as

$$F_{Z1} = F_{Z2} = \frac{mgL_r}{2(L_f + L_r)}, \tag{2.16}$$

$$F_{Z3} = F_{Z4} = \frac{mgL_f}{2(L_f + L_r)}, \tag{2.17}$$

$$\alpha_{1,2} = \delta_1 - \beta - \frac{L_f r}{V}, \tag{2.18}$$

and

$$\alpha_{3,4} = \delta_2 - \beta + \frac{L_r r}{V}. \tag{2.19}$$

Finally, lateral displacement, Y, of the CG obeys the following dynamics of motion [6]

$$\dot{Y} = V sin(\beta + \psi), \tag{2.20}$$

where $\psi \in \Re$ refers to the yaw angle.

2.2 Unstable Vehicle Motions

2.2.1 Understeer

During understeer, front tires of a vehicle lose their grip on the road and start slipping. This happens when the driver is cornering with high acceleration/deceleration. The front tires hit their lateral force saturation limit and start slipping. Front tires turn less than the desired amount because of slippage and the car's front end is pushed outside of the corner. The car turns with a larger radius compared to the driver's intended path. This is a condition in which the front tires' slip angle is larger than that of the rear tires ($|\alpha_f| > |\alpha_r|$).

2.2.2 Oversteer

During oversteer, rear tires lose their grip on the road, the back end of the car is pushed outside of the corner. This condition is common in powerful rear-wheel drive vehicles, where the rear tires reach to their grip-limit earlier than the front tires and start slipping, pushing the front end of the vehicle inside the corner. The car steers more sharply than desired and thus turns with a smaller radius of curvature. This is a condition in which rear tires' slip angle is larger than the front tires' slip angle ($|\alpha_r| > |\alpha_f|$).

It is noted that oversteer is not limited to rear-wheel drive vehicles only.

2.2.3 Fishtailing

Fishtailing is an uncontrolled oversteer. During fishtailing rear tires lose traction on the road and start to skid sideways causing the rear end of the vehicle to swing behind the front end (see Fig. 2.2). During fishtailing, when car's back end slides in one direction, it must be corrected by counter-steering. This can be achieved by aligning the tires in the direction of skid so that they can rotate freely to match the vehicle speed. This counter-steering action eventually reduces the tire slip angles and lateral tires forces. However, over-correction by the driver can make the rear end of the vehicle to skid in the opposite direction and can push the vehicle into persistent oscillations.

2.3 Background and Creating Fishtailing

If the tires stop rolling and start sliding, the stability of the vehicle may be lost. While tire is rolling in longitudinal direction or cornering, it should provide traction forces and cornering forces. The resultant of longitudinal and lateral forces can not be greater than the limit set by the friction. During cornering, a tire experiences tire slip angle and as a result lateral tire force is generated.

Lateral tire force increases with the increasing tire slip angle upto a certain threshold value ($\approx 5^o$), and beyond that angle, lateral tire force can not increase and reaches to its saturation value determined by road friction. In the sections below, the tire slip angle and causes of fishtailing motion are discussed.

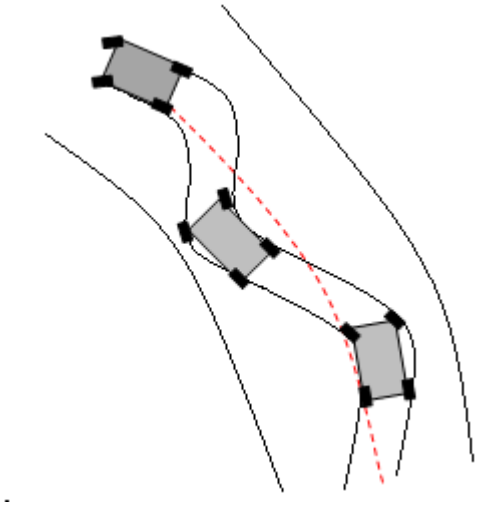

Figure 2.2: Car fishtailing on curved road

2.3.1 Tire Slip Angle, α

This is the angle, α, between the wheel pointing direction and the direction the wheel is travelling towards. α can be observed in Fig. 2.3 [30].

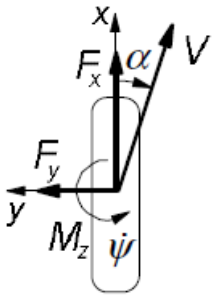

Figure 2.3: Tire slip angle, α.

2.3.2 Causes of Tire Slip Angle

If a vehicle is travelling in a direction other than its pointing direction, it means it is sliding. A sideways load imposed against the tires causes their velocity vectors to point at a certain angle w.r.t their pointing direction and gives rise to tire slip angles. This sideways load is due to vehicle inertia during cornering and the centrifugal force is the representation of this effect which resists the car motion in a curved path. Therefore, there are two major causes of the slip angle:

1. Steering angle of the wheel.
2. Centrifugal force (due to vehicle inertia during cornering).

Centrifugal force is the representation of car inertia during cornering that resists the car motion in curved path. Centrifugal force is the force that pushes the vehicle outside of the corner while on the other hand, cornering force is the force generated by tires-road friction interaction that pulls the vehicle in the direction of travel to follow the desired path (see Fig. 2.4). Given enough friction, tires are able to prevent this centrifugal force effect. However, if car is going on a slippery road at a high velocity carrying high momentum, a sudden cornering or steering action will make the wheels develop large slip angles and corresponding large lateral forces. If these forces reach their saturation limits while making an effort to overcome the centrifugal force effect, the vehicle slides out of the corner.

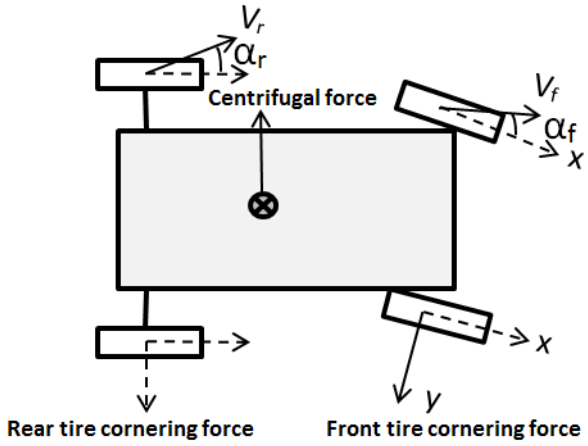

Figure 2.4: Tire slip angles and lateral tire forces.

2.3.3 How $\alpha_r > \alpha_f$ condition, observed in fishtailing, is developed?

The condition of rear slip angle being greater than the front slip angle, $\alpha_r > \alpha_f$, depends on two major factors given below:

- Weight distribution
- Location of vehicle center of gravity

A vehicle having a center of gravity (cog) close to the rear end experiences more centrifugal force effect at the rear compared to the front. This centrifugal force effect causes more tire deflection at rear tires in tire-road contact patch area and hence slip angle generated at rear tires becomes larger than the front tires' slip angle. The driver having direct steering control over front tires is also a contributing factor for the smaller front tire slip angle since the driver can adjust his/her steering to reduce slippage. Under these conditions, the vehicle experiences oversteer, which is represented by the condition $\alpha_r > \alpha_f$.

2.3.4 Creating Fishtailing

Vehicle Configuration used for creating fishtailing is given in Fig. 2.5 [27]. It can be observed in Fig. 2.5 that the center of gravity (cog) is close to rear end and hence $L_r < L_f$. Lateral tire forces, F_{Yi}, normal loads, F_{Zi}, and tire slip angles, α_i, $i = 1, 2, 3, 4$, are given as

$$F_{Yi} = C_\alpha \alpha_i F_{Zi} = C_i \alpha_i, \tag{2.21}$$

$$F_{Z1,2} = \frac{mgL_r}{2(L_f + L_r)}, \tag{2.22}$$

$$F_{Z3,4} = \frac{mgL_f}{2(L_f + L_r)}, \tag{2.23}$$

$$\alpha_{1,2} = \delta_1 - \beta - \frac{L_f r}{V}, \tag{2.24}$$

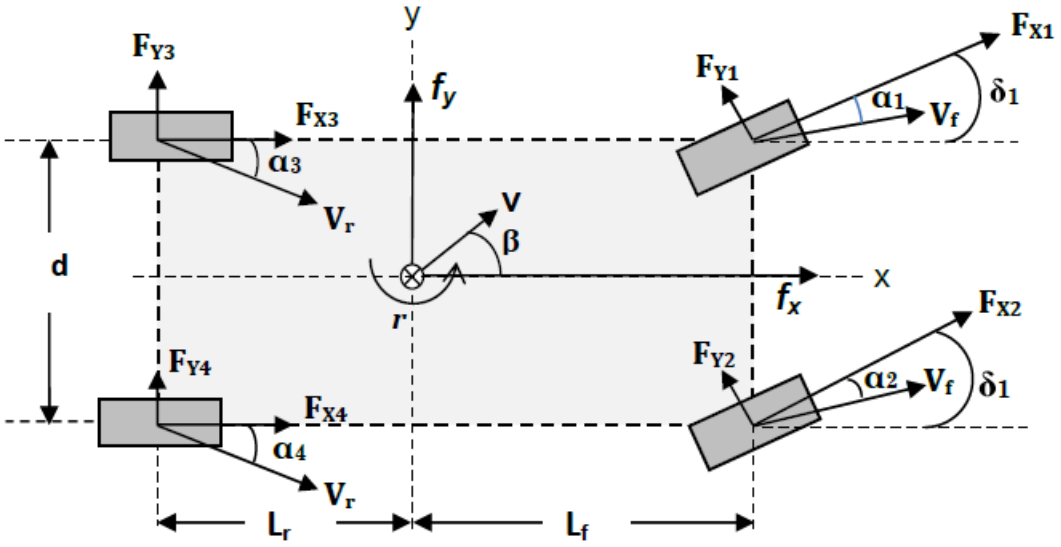

Figure 2.5: Vehicle configuration.

and

$$\alpha_{3,4} = \delta_2 - \beta + \frac{L_r r}{V} = -\beta + \frac{L_r r}{V}. \tag{2.25}$$

C_i in (2.21) is the cornering stiffness of the i^{th} tire and calculated as $C_i = C_\alpha F_{Zi}$. Cornering stiffness coefficient, C_α, is the same for all four tires. However, since L_r is smaller than L_f, $F_{Z1,2} < F_{Z3,4}$, based on (2.22) and (2.23). Hence, front tires' cornering stiffness, $C_{1,2} = C_\alpha F_{Z1,2}$, is smaller than rear tires' cornering stiffness, $C_{3,4} = C_\alpha F_{Z3,4}$. This means that rear tires' force development with increasing tire slip angle, is larger compared to that of front tires. Therefore, rear tire forces reach their saturation limits earlier and once they hit the saturation, further increase in rear tires slip angles causes skidding sideways.

The effects of the driver steering angles, δ_i, $i = 1, 2$, cog slip angle, β, and the distance of cog from the front and rear ends, L_f and L_r, can be seen in (2.24) and (2.25).

Having higher slip angles at the rear compared to the front of the vehicle, combined with pure gain driver model and high driver throttle input, forms the fishtailing motion in the simulations. The vehicle parameters used for creating fishtailing motion is given in following Table 2.2.

Table 2.2: Vehicle parameters used in simulation.

m	1300 $[kg]$
g	9.81 $[m/s^2]$
L_f	1.3 $[m]$
L_r	1.2 $[m]$
d	1.6 $[m]$
C_α (Asphalt)	13.178 $[1/rad]$
C_α (Snow)	5.27 $[1/rad]$
J_z	1300 $[kgm^2]$
V_o	16 $[m/s]$

Chapter 3

Proposed Control Allocation Method

3.1 Control Allocation to Recover from Driver Induced Oscillations

The objective of the control allocation is to obtain the actual control inputs, u; front steering correction angle, rear steering angle and longitudinal traction forces which will give rise to virtual/reference control inputs, v. To make the vehicle model suitable for control allocation implementation, virtual control inputs, v, need to be linked with actual control inputs, u. The relation is defined as $v = g(u)$, where $g : \mathcal{R}^m \mapsto \mathcal{R}^k$ is mapping of actual control inputs to virtual control inputs and m (number of actual control inputs) $> k$ (number of virtual control inputs). The major part of control allocation literature engages the linear case where actual control inputs are linked with virtual control inputs by linear relation, $v = Bu$. And B is known as control effectiveness matrix. To obtain control effectiveness matrix, B, nonlinear vehicle model from Chapter 2 needs to be linearized. In the following section, linearized vehicle model is obtained in order to determine B matrix for control allocation implementation.

3.1.1 Linearized State Space Model

Longitudinal and lateral forces in (2.3)-(2.10) are linearized around a constant velocity V_o by assuming small steering and side slip angles. Hence, (2.3)-(2.10) reduces to

$$F_{x,fl} = F_{X1}, \tag{3.1}$$

$$F_{x,fr} = F_{X2}, \tag{3.2}$$

$$F_{x,rl} = F_{X3}, \tag{3.3}$$

$$F_{x,rr} = F_{X4}, \tag{3.4}$$

$$F_{y,fl} = F_{Y1} = C_\alpha(\delta_1 - \beta - \frac{L_f r}{V_o})F_{Z1}, \tag{3.5}$$

$$F_{y,fr} = F_{Y2} = C_\alpha(\delta_1 - \beta - \frac{L_f r}{V_o})F_{Z2}, \tag{3.6}$$

$$F_{y,rl} = F_{Y3} = C_\alpha(\delta_2 - \beta + \frac{L_r r}{V_o})F_{Z3}, \tag{3.7}$$

and

$$F_{y,rr} = F_{Y4} = C_\alpha(\delta_2 - \beta + \frac{L_r r}{V_o})F_{Z4}. \tag{3.8}$$

Similarly, (2.20) is linearized as

$$\dot{Y} = V_o(\beta + \psi). \tag{3.9}$$

Using (2.1)-(2.2), (2.11)-(2.14) and (3.1)-(3.9), the non-linear 2-track model can be linearized and represented in state space form as

$$\dot{X} = AX + B_u u_n, \tag{3.10}$$

where $X = \begin{bmatrix} Y & V & \beta & \psi & r \end{bmatrix}^T$, $u_n = \begin{bmatrix} \delta_1 & \delta_2 & F_{X1} & F_{X2} & F_{X3} & F_{X4} \end{bmatrix}^T$,

$$A = \begin{bmatrix} 0 & 0 & V_o & V_o & 0 \\ 0 & 0 & 0 & 0 & 0 \\ 0 & 0 & -\frac{2C_\alpha(F_{Z1}+F_{Z3})}{mV_o} & 0 & \frac{2C_\alpha(L_r F_{Z3} - L_f F_{Z1})}{mV_o^2} - 1 \\ 0 & 0 & 0 & 0 & 1 \\ 0 & 0 & \frac{2C_\alpha(L_r F_{Z3} - L_f F_{Z1})}{J_z} & 0 & -\frac{2C_\alpha(F_{Z1}L_f^2 + F_{Z3}L_r^2)}{J_z V_o} \end{bmatrix}, \tag{3.11}$$

and

$$B_u = \begin{bmatrix} 0 & 0 & 0 & 0 & 0 & 0 \\ 0 & 0 & \frac{1}{m} & \frac{1}{m} & \frac{1}{m} & \frac{1}{m} \\ \frac{2C_\alpha F_{Z1}}{mV_o} & \frac{2C_\alpha F_{Z3}}{mV_o} & 0 & 0 & 0 & 0 \\ 0 & 0 & 0 & 0 & 0 & 0 \\ \frac{2C_\alpha F_{Z1} L_f}{J_z} & -\frac{2C_\alpha F_{Z3} L_r}{J_z} & -\frac{d}{2J_z} & \frac{d}{2J_z} & -\frac{d}{2J_z} & \frac{d}{2J_z} \end{bmatrix}. \tag{3.12}$$

During fishtailing, the driver tries to keep the front end of the vehicle at the center of the lane. The output of the overall closed loop system, Y_f, is then defined as the lateral deviation of front end of vehicle from the lane center as

$$Y_f = Y + L_f sin(\psi), \tag{3.13}$$

where $Y \in \Re$ is lateral displacement of car COG. Using the small angle assumption, (3.13) can be linearized as

$$Y_f = Y + L_f \psi.$$

Therefore, the output equation can be written as $Y_f = CX$, where $C = \begin{bmatrix} 1 & 0 & 0 & L_f & 0 \end{bmatrix}$.

3.2 Problem Formulation and Solution

In the proposed control structure (see Fig. 3.1), the driver controls the front steering angle input, $\delta_{driver} \in \Re$, and the throttle. These driver inputs are converted to reference forces and moments acting on the vehicle, via a "Reference Generator". The control allocation, then, provides the front steering angle correction, $\Delta\delta_1 \in \Re$, rear steering angle, $\delta_2 \in \Re$, and traction forces F_{Xi}, $i = 1, 2, 3, 4$, to realize the reference forces and moments. To indicate the roles of the driver and the control allocator separately on determining the control input, u_n, (3.10) is rewritten as

$$\dot{X} = AX + B_u(u + \Delta u), \tag{3.14}$$

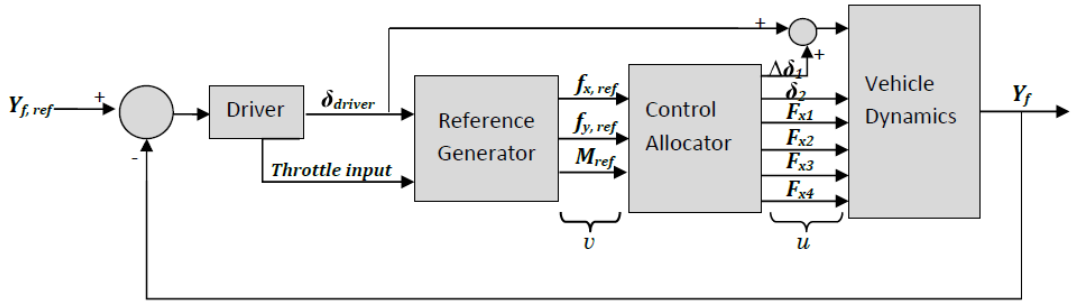

Figure 3.1: Overall control structure.

where $u = \begin{bmatrix}\Delta\delta_1 & \delta_2 & F_{X1} & F_{X2} & F_{X3} & F_{X4}\end{bmatrix}^T$ and $\Delta u = \begin{bmatrix}\delta_{driver} & 0 & 0 & 0 & 0 & 0\end{bmatrix}^T$. Since $B_u \in \mathcal{R}^{5\times 6}$ is rank deficient, i.e. $rank(B_u) = 3 < 6$, it can be decomposed into two matrices as

$$B_u = B_v B, \tag{3.15}$$

where $B_v \in \mathcal{R}^{5\times 3}$ and $B \in \mathcal{R}^{3\times 6}$ have rank 3. Substituting (3.15) in (3.14), it is obtained that

$$\begin{aligned}\dot{X} &= AX + B_v B(u + \Delta u), \\ &= AX + B_v v,\end{aligned} \tag{3.16}$$

where $v = B(u + \Delta u)$. $v \in \mathcal{R}^3$ is the vector containing the desired forces and moments, generated by the reference generator according to driver's intentions (see Fig. 3.1). $B(u + \Delta u) \in \Re^3$, on the other hand, is the model of the achieved forces and moments. $B_v \in \mathcal{R}^{5\times 3}$ and $B \in \mathcal{R}^{3\times 6}$ can be formed as

$$B_v = \begin{bmatrix} 0 & 0 & 0 \\ \frac{1}{m} & 0 & 0 \\ 0 & \frac{1}{mV_o} & 0 \\ 0 & 0 & 0 \\ 0 & 0 & \frac{1}{J_z} \end{bmatrix}, \tag{3.17}$$

and

$$B = \begin{bmatrix} 0 & 0 & 1 & 1 & 1 & 1 \\ C_\alpha(2F_{Z1}) & C_\alpha(2F_{Z3}) & 0 & 0 & 0 & 0 \\ C_\alpha L_f(2F_{Z1}) & -C_\alpha L_r(2F_{Z3}) & -\frac{d}{2} & \frac{d}{2} & -\frac{d}{2} & \frac{d}{2} \end{bmatrix}. \tag{3.18}$$

The objective of a conventional control allocator is to achieve $v = B(u + \Delta u)$ by manipulating u. The goal of the proposed control allocation, on the other hand, is not only to realize the desired forces and moments vector, v, by ensuring $v = B(u + \Delta u)$, but also to synchronize these two signals, v and $B(u + \Delta u)$, to eliminate the time delay introduced due to the phase shift shown in Fig. 1.2. How this is achieved is explained in the following sections by first describing the creation of desired/reference forces and moments and then introducing the proposed control allocation algorithm.

3.2.1 Reference Forces and Moments

Vector v consists of the desired forces and moments on the vehicle, determined by the steering and throttle inputs from the driver. Namely, $v = \begin{bmatrix} f_{x,ref} & f_{y,ref} & M_{ref} \end{bmatrix}^T$, where $f_{x,ref}$, $f_{y,ref}$ and M_{ref} are the total reference longitudinal force, total reference lateral force and the reference yaw moment, respectively. Below, calculation of these reference forces and moments are explained.

3.2.1.1 Reference Yaw Moment (M_{ref})

Reference yaw moment can be obtained from the relationship

$$M_{ref} = J_z \dot{r}_{ref}, \tag{3.19}$$

where r_{ref} is the reference yaw rate, which can be calculated using the single track representation given in Fig. 3.2 [31]. The equations of motion obtained

from this representation are given as

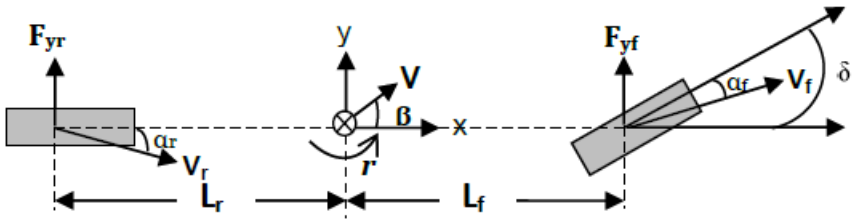

Figure 3.2: Linear single track model.

$$\dot{\beta} = (-1 + \frac{(C_r L_r - C_f L_f)}{mv^2})r + (\frac{-C_f - C_r)}{mv})\beta + (\frac{C_f}{mv})\delta_f,$$
$$\dot{r} = (\frac{-C_r L_r^2 - C_f L_f^2}{J_z v})r + (\frac{C_r L_r - C_f L_f}{J_z})\beta + (\frac{C_f L_f}{J_z})\delta_f, \tag{3.20}$$

where $C_f \in \Re$ and $C_r \in \Re$ are front and rear cornering stiffnesses, respectively. Assuming that the conditions $\dot{\beta} = 0$ and $\dot{r} = 0$ provide a desirable driving condition and solving (3.20) for r_{ref}, it is obtained that

$$r_{ref} = \frac{V}{(L_f + L_r) + k_{us} V^2}\delta_f, \tag{3.21}$$

where

$$k_{us} = \frac{m(L_r C_r - L_f C_f)}{(L_f + L_r)C_f C_r}. \tag{3.22}$$

In (3.22), assuming that the front two tires are merged into single tire at front axle and rear two tires into single tire at rear axle, C_f and C_r can be calculated as $C_f = 2C_\alpha F_{Z1}$ and $C_r = 2C_\alpha F_{Z3}$. It is noted that in C_f and C_r calculations, the assumptions $F_{Z1} = F_{Z2}$ and $F_{Z3} = F_{Z4}$ are used.

3.2.1.2 Reference Longitudinal Force ($f_{x,ref}$)

Reference longitudinal force is determined directly by the driver throttle input per tire, F_{xi}, $i = 1, 2, 3, 4$, and thus calculated as

$$f_{x,ref} = 4F_{xi}. \tag{3.23}$$

3.2.1.3 Reference Lateral Force ($f_{y,ref}$)

Assuming that the driver prefers a zero side slip derivative, $\dot{\beta} = 0$, and substituting this condition into (2.12), $f_{y,ref}$ can be obtained as

$$f_{y,ref} = \frac{mVr_{ref} + f_{x,ref}sin(\beta)}{cos(\beta)}. \tag{3.24}$$

3.2.2 Control Allocation Algorithm

In conventional control allocation approaches, the error between the reference and achieved control inputs are minimized by first defining a cost function

$$J = \|B(u + \Delta u) - v\|_2^2 + \epsilon \|u\|_2^2, \tag{3.25}$$

where $0 \leq \epsilon \leq 1$, and then solving for u using standard optimization algorithms. The proposed control allocation method, on the other hand, synchronizes v and $B(u + \Delta u)$ to eliminate the phase shift between these signals to help the vehicle recover from the fishtailing event. The synchronization is achieved by adding a derivative error minimization term to the objective function, which results in

$$J = \|B(u + \Delta u) - v\|_2^2 + \left\|\Gamma_d[B(\dot{u} + \dot{\Delta u}) - \dot{v}]\right\|_2^2 + \epsilon \|u\|_2^2, \tag{3.26}$$

where $\Gamma_d \in R^{3\times3}$ is a weighting matrix. Expressing the 2-norm as $\|X\|_2^2 = X^T X$, and after approximating $\dot{u}[kT]$ as $\{u[kT]-u[(k-1)T]\}/T$, where T is the sampling interval and k is an integer, (3.26) can be rewritten as

$$\begin{aligned} J =& u^T[B^TQB + B^TT^2B + \epsilon I]u + 2[\Delta u^T B^T T^2 B + \dot{\Delta u}^T B^T TQB - v^T T^2 B - \\ & \dot{v}^T TQB - u^{-T} B^T QB]u + v^T T^2 v + \dot{v}^T T^2 Q\dot{v} + \Delta u^T B^T T^2 B\Delta u + \\ & \dot{\Delta u}^T B^T T^2 QB\dot{\Delta u} + u^{-T} B^T QBu^- + 2\dot{v}^T TQBu^- - 2\dot{\Delta u}^T B^T TQBu^- \\ & - 2\dot{v}^T T^2 QB\dot{\Delta u} - 2v^T T^2 B\Delta u, \end{aligned} \tag{3.27}$$

where $Q = \Gamma_d^T \Gamma_d$, and $I \in \mathcal{R}^{6\times6}$ is an identity matrix. Defining

$$\begin{aligned} P =& 2[B^TQB + B^TT^2B + \epsilon I], \\ H^T =& 2[\Delta u^T B^T T^2 B + \dot{\Delta u}^T B^T TQB - v^T T^2 B - \dot{v}^T TQB - u^{-T} B^T QB], \end{aligned}$$

and

$$C = v^T T^2 v + \dot{v}^T T^2 Q \dot{v} + \Delta u^T B^T T^2 B \Delta u + \dot{\Delta u}^T B^T T^2 Q B \dot{\Delta u} + u^{-T} B^T Q B u^- + 2\dot{v}^T T Q B u^- - 2\dot{\Delta u}^T B^T T Q B u^- - 2\dot{v}^T T^2 Q B \dot{\Delta u} - 2 v^T T^2 B \Delta u,$$

(3.27) can be expressed as

$$J = \frac{1}{2} u^T P u + H^T u + C. \tag{3.28}$$

Minimizing (3.28) is equivalent to minimizing $J = \frac{1}{2} u^T P u + H^T u$, which can be performed by using readily available software packages, such as Matlab quadratic programming function.

3.2.2.1 Position and Rate Constraints on the Control Input Vector

The control input vector, $u = \begin{bmatrix} \Delta\delta_1 & \delta_2 & F_{X1} & F_{X2} & F_{X3} & F_{X4} \end{bmatrix}^T$, produced by the control allocator, needs to satisfy the position and rate constraints

$$u_{min} \leq u(t) \leq u_{max} \tag{3.29}$$

$$\dot{u}_{min} \leq \dot{u}(t) \leq \dot{u}_{max} \tag{3.30}$$

$\dot{u}(t)$ can be approximated as $\dot{u}(t) \approx \{u(t) - u(t-T)\}/T$, where T is the sampling time. Using derivative approximation, rate constraint (3.30) can be rewritten as the position constraint

$$u(t-T) + T\dot{u}_{min} \leq u(t) \leq u(t-T) + T\dot{u}_{max}. \tag{3.31}$$

Using (3.29) and (3.31), and defining $\dot{u}_{min} = \Delta u_{min}/T$ and $\dot{u}_{max} = \Delta u_{max}/T$, the combined position and rate limits on the control signals can be defined as

$$\underline{u}(t) \leq u(t) \leq \overline{u}(t), \tag{3.32}$$

where

$$\underline{u}(t) = max\{u_{min}, u(t-T) + \Delta u_{min}\}, \tag{3.33}$$

$$\overline{u}(t) = min\{u_{max}, u(t-T) + \Delta u_{max}\}. \tag{3.34}$$

For the vehicle model that will be simulated in this paper, the saturation variables are taken as [13]

$$u_{max} = \begin{bmatrix} 5^o & 5^o & 250N & 250N & 250N & 250N \end{bmatrix}^T,$$
$$u_{min} = \begin{bmatrix} -5^o & -5^o & 50N & 50N & 50N & 50N \end{bmatrix}^T,$$
$$\Delta u_{max} = \begin{bmatrix} 0.5^o & 0.5^o & 0.5N & 0.5N & 0.5N & 0.5N \end{bmatrix}^T$$

and

$$\Delta u_{min} = \begin{bmatrix} -0.5^o & -0.5^o & -0.5N & -0.5N & -0.5N & -0.5N \end{bmatrix}^T.$$

During the simulations, the sampling interval is taken as $T = 20ms$.

3.3 Simulation Results

In this section, the effectiveness of the proposed control allocation (CA) method to prevent driver induced oscillations (DIO) is demonstrated. Increasingly challenging operating conditions are introduced to show that when the conditions are favorable, alternative solutions provide satisfactory performance, but when the circumstances become unfavorable, these alternative solutions fail and the proposed approach proves to be useful to recover stability. Firstly, the vehicle is tested with driver control only, without the help of any auxiliary controller. This test can also be interpreted as a fixed CA case, where the driver input is converted to steering and traction inputs directly, without any optimization process. It is shown that in this configuration, the task of keeping the car on the lane center can be achieved on an asphalt road but the vehicle tends to enter into a DIO when the road friction decreases, for example in the presence of snow. Second, a conventional optimization based CA is introduced to the system which augments the driver and it is demonstrated that this new control configuration can recover the vehicle from DIO. Third, it is shown that in even more challenging operating conditions, for example high speed on a snow-covered road, the conventional

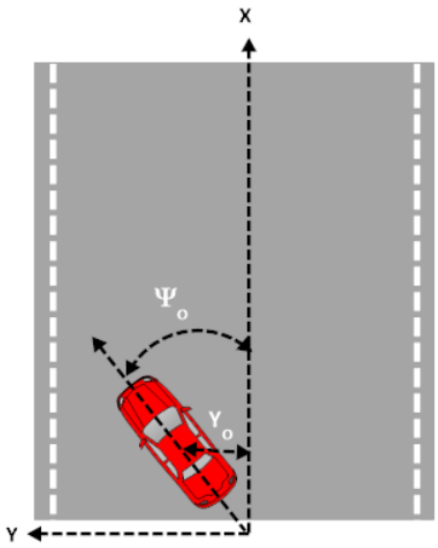

Figure 3.3: The initial orientation of the vehicle.

CA also becomes insufficient. Finally, for these operating conditions, where conventional CA fails, the proposed CA method is shown to be able to recover the stability of the system.

In all the simulations, the vehicle starts with an initial speed of 16m/s and an initial orientation where the center of gravity is slightly shifted from the lane center and the vehicle's nose is directed away from the center (see Fig. 3.3). It is shown in [32] that in pilot induced oscillations, pilots behave like a pure gain. Since a similar phenomenon is being investigated here, a pure gain driver model is used. This is not central to the development of the proposed method and other driver models can also be employed. The full nonlinear vehicle model used in the simulations is explained in (2.1)-(2.20). The linearized model (3.16) is used only for the control allocation design. Below, vehicle tests with increasing difficulty, in terms of operating conditions, are explained in detail with different control allocation structures.

3.3.1 Fixed Control Allocation Augmentation

In this scenario, the driver manipulates the front steering angle, δ_1, and provides a constant torque input, T_{driver}, of 325 Nm. The CA directly transfers the steering input to the front tires and equally distributes the traction force to each tire. Rear steering is not used, and thus $\delta_2 = 0$. Two road conditions, *asphalt* and *snow-covered*, are tested. These conditions are introduced by setting the cornering stiffness coefficients to 13.178[1/rad] and 5.27[1/rad], for the asphalt and snow-covered cases, respectively [33].

Starting with the initial conditions explained above and depicted in Fig. 3.3, driver inputs and the evolution of vehicle states in asphalt and snow-covered cases are shown in Fig. 3.4. The driver gives steering input to offset the initial lateral displacement of the car front end from the hypothetical center-line of the lane. However, large steering input at a high velocity gives rise to the development of side slip angle, β. As seen from the figures, the vehicle enters into a persistent oscillation pattern on the snow-covered road, whereas the oscillations die out rather quickly on the asphalt road. The reasons for this behavior can be better understood from the results shown in Fig. 3.5. Due to the low friction on the snow-covered road, lateral tire forces reaches their saturation limits quickly and starts skidding. As explained earlier, this causes a sluggish response to driver commands and thus makes the driver give stronger compensating steering inputs, which makes the situation worse and causes sustained oscillations, which is a very similar phenomenon to pilot induced oscillations [1, 2].

When the front and rear tire lateral forces and tire slip angles are investigated closely for the snow-covered case, in Fig. 3.5b and Fig. 3.5d, a typical pattern observed during fishtailing events can be seen: It is mostly the rear tires that skid, while the front tires operate within their saturation limits, after an initial skidding period. This causes a "tail oscillation", which is also depicted in Fig. 1.1.

It is noted that the longitudinal velocity keeps increasing in both the asphalt and snow-covered roads (see Fig. 3.4b) due to the constant throttle input. However, this increase in velocity is more prominent on asphalt, since the resulting

longitudinal force on snow-covered road is dramatically diminished due to large oscillations.

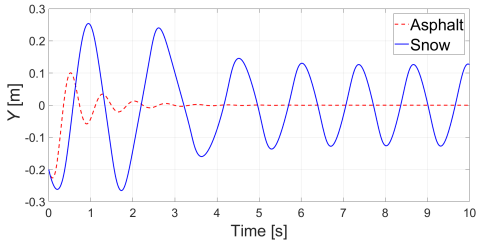

(a) Lateral displacement of the car center of gravity, Y

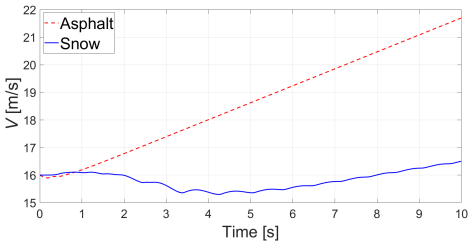

(b) Longitudinal velocity, V

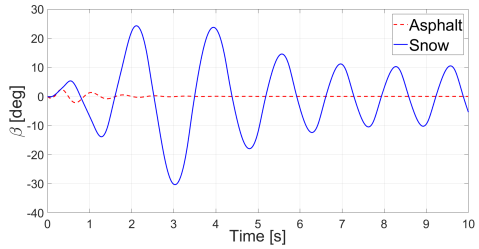

(c) Side slip angle, β

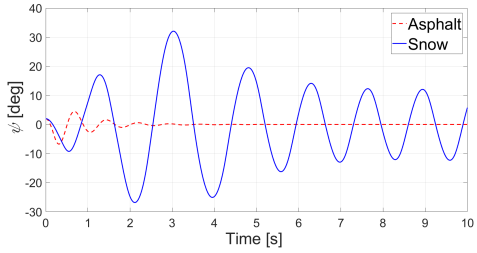

(d) Yaw angle, ψ

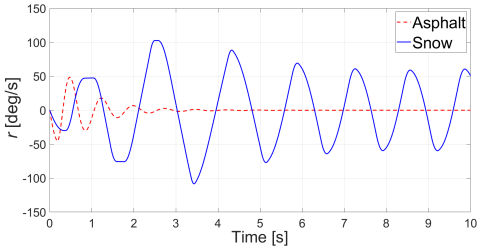

(e) Yaw rate, r

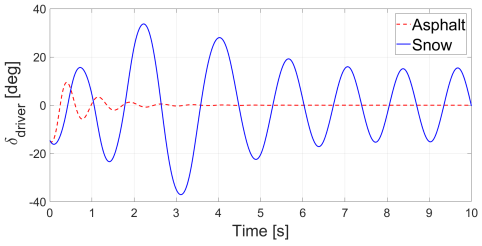

(f) Driver steering angle input, δ_{driver}

Figure 3.4: Evolution of the vehicle states and the driver steering input in asphalt and snow-covered roads in the case of fixed control allocation.

Although the desired/reference forces and moments vector, v (see Fig. 3.1), is not used for the derivation of fixed control allocation outputs, it is calculated and compared with the achieved forces and moments to demonstrate how much of the driver intent is actually realized on the asphalt and snow-covered roads. It is seen in Fig. 3.6 that on asphalt road, the desired longitudinal and later forces, as well as the yaw moment, are tracked reasonably well by the vehicle. However, Fig. 3.6b demonstrates that on the snow-covered road the net longitudinal force keeps oscillating due to oscillations in both the side slip angle, β, and lateral tire

forces. In Fig. 3.6d, it can be seen that the net lateral force is much smaller compared to the desired lateral force due to the saturation limits caused by the low friction of the snow-covered road. Fig. 3.6f also demonstrates the oscillating achieved-yaw-moment together with its phase shift compared to the desired-yaw-moment, which is an indicator of effective time delay in the loop, instigating persistent oscillations.

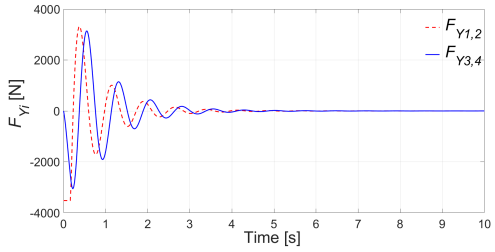

(a) Lateral tire forces, F_{Yi} (Asphalt)

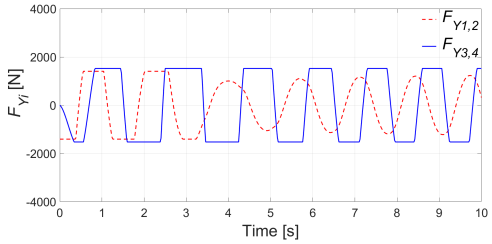

(b) Lateral tire forces, F_{Yi} (Fully Snow)

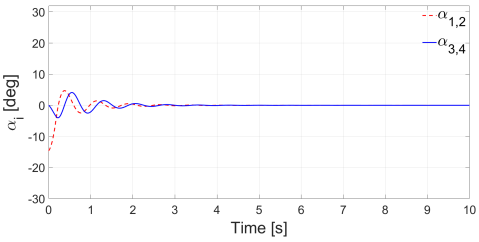

(c) Tire slip angles, α_i (Asphalt)

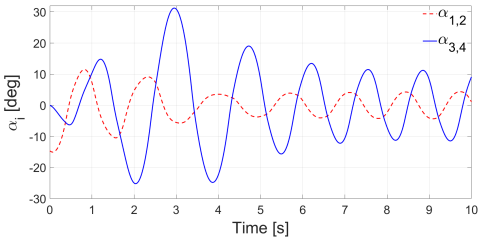

(d) Tire slip angles, α_i (Fully Snow)

Figure 3.5: Lateral tire forces and slip angles on asphalt and snow-covered roads in the case of fixed control allocation.

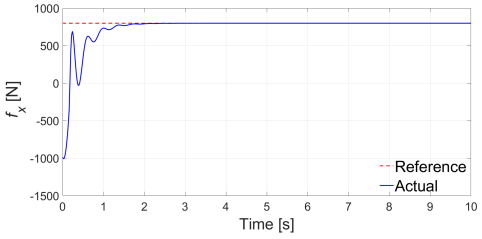

(a) Reference vs. actual longitudinal force (Asphalt)

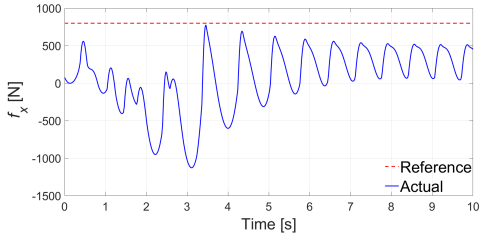

(b) Reference vs. actual longitudinal force (Fully Snow)

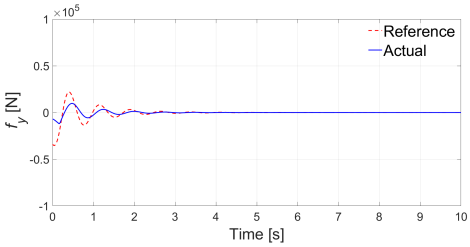

(c) Reference vs. actual lateral force (Asphalt)

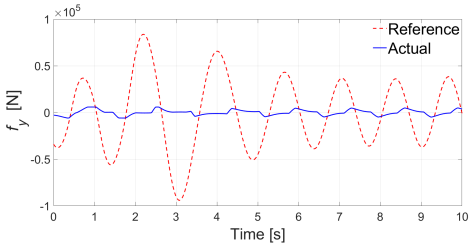

(d) Reference vs. actual lateral force (Fully Snow)

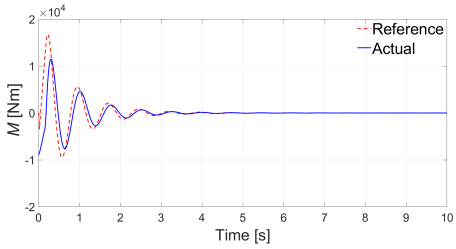

(e) Reference vs. actual yaw moment (Asphalt)

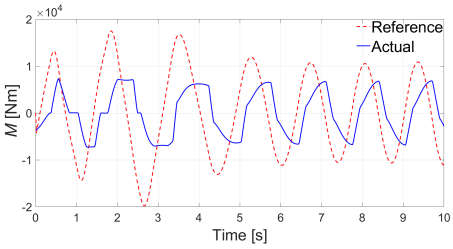

(f) Reference vs. actual yaw moment (Fully Snow)

Figure 3.6: Comparison of virtual and actually achieved forces and moments in asphalt and snow cases (Fixed control allocation).

3.3.2 Conventional Optimal Control Allocation Augmentation

In the second scenario, the optimal control allocation, which minimizes the cost function (3.25), is used to map the driver intentions to front steering angle correction, $\Delta\delta_1$, rear steering angle, δ_2, and traction forces in each wheel, $F_{Xi}, i = 1, 2, 3, 4$. The scenario starts with the same initial conditions and the same fixed CA used in the previous section and the optimal CA is activated only after the vehicle enters into a DIO. Two different time instants are used for switching from fixed CA to conventional CA, and therefore two sub-scenarios are investigated. In the first sub-scenario, switching occurs at $t = 13s$ and in the second one at $t = 15s$. The main difference between these two cases is the speed of the vehicle at the time of switching, which effects the performance of the optimal CA. To make the scenarios more challenging, snow-covered road conditions (low friction) are used.

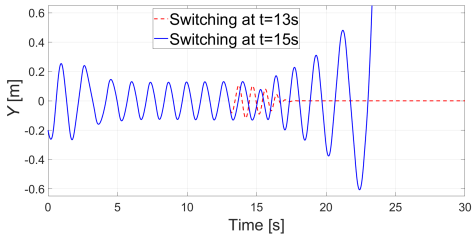

(a) Lateral displacement of the car center of gravity, Y.

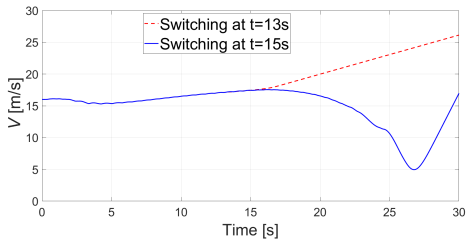

(b) Longitudinal velocity, V

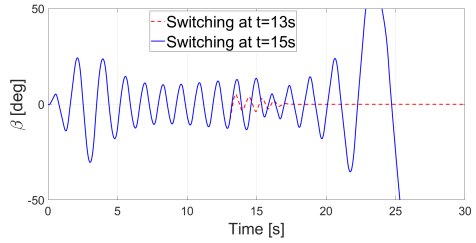

(c) Side slip angle, β

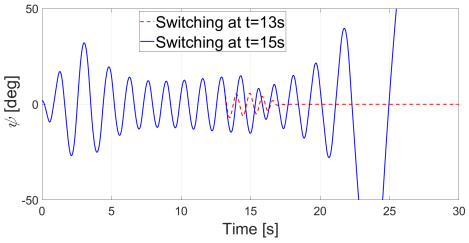

(d) Yaw angle, ψ

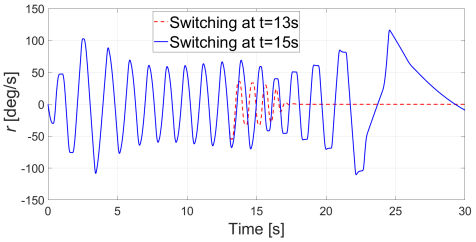

(e) Yaw rate, r

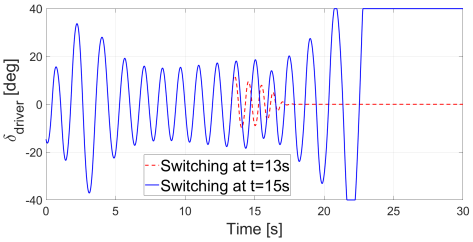

(f) Driver steering angle input, δ_{driver}

Figure 3.7: Evolution of system states and the driver steering input for two different switching times: The exploited control allocation (CA) is switched from the fixed CA to a conventional optimal CA at t=13s in one case and at t=15s, in the other, resulting in dramatically different system responses.

Fig. 3.7 shows the time evolution of system states and the driver input for two different switching times. When switching occurs at $t = 13s$, the optimal CA is able to recover the vehicle from the DIO. On the other hand, when the optimal CA is activated at $t = 15s$, the states continues to oscillate and grows in an unbounded manner. When successful, for the former switching time, optimal CA helps the vehicle recover from the DIO since it prevents side slip variations by enforcing the condition $\dot{\beta} = 0$. When switching occurs at $t = 15s$, however, this can not be achieved since at the time of switching the velocity of the vehicle is higher and actuators are more prone to saturation. The difference between the CA outputs for two different switching instances can be seen in Fig. 3.8. It is

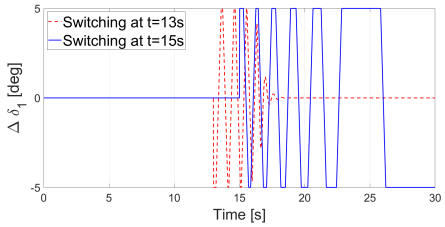

(a) Front steering correction angle, $\Delta\delta_1$

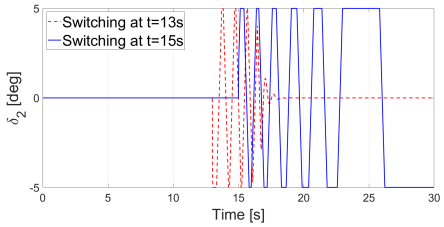

(b) Rear steering angle, δ_2

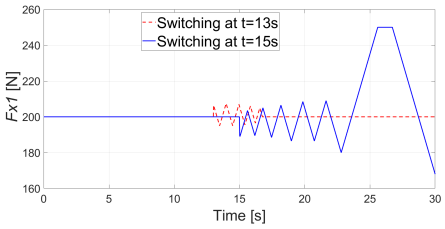

(c) Front left tire's longitudinal force, F_{X1}

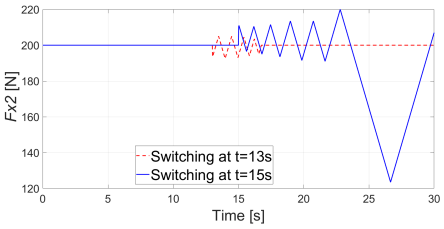

(d) Front right tire's longitudinal force, F_{X2}

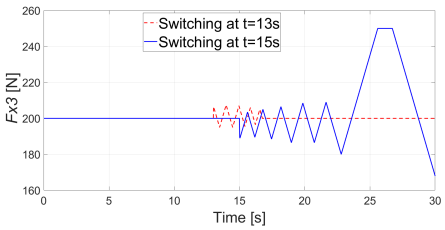

(e) Rear left tire's longitudinal force, F_{X3}

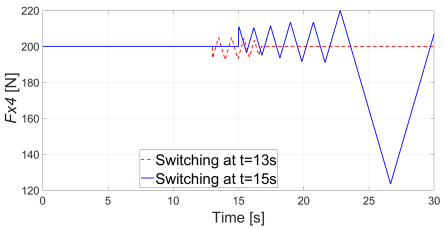

(f) Rear right tire's longitudinal force, F_{X4}

Figure 3.8: Evolution of control allocation (CA) outputs for two different switching times: The exploited control allocation (CA) is switched from the fixed CA to a conventional optimal CA at t=13s in one case and at t=15s, in the other.

noted that when the optimal CA is activated at $t = 13s$, it is able to help the driver by aligning the tires in the direction of side slip, which eventually reduces the tire slip angles and the corresponding tire lateral forces (see Fig. 3.9). The movement of the tires that become aligned with the slip direction is depicted in Fig. 3.10. Once the lateral forces and slip angles decrease, tires start gaining traction and the vehicle recovers stability.

The reference/desired and achieved/actual forces and moments are depicted in Fig. 3.11, for two switching times. Consistent with the earlier observations, $t = 13s$ switching helps the vehicle follow the driver's desired forces and moments, while the vehicle struggles to obey driver's commands when switching occurs at

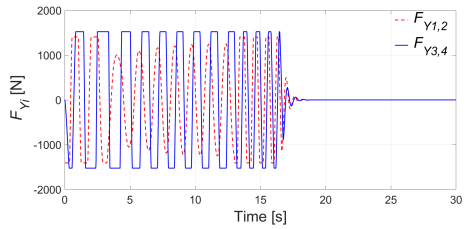

(a) Lateral tire forces, F_{Yi} (Switching at t=13 seconds)

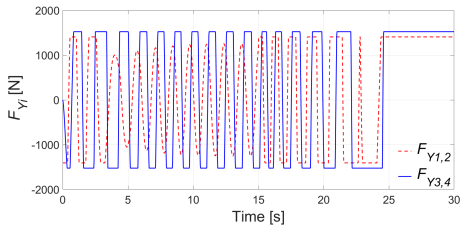

(b) Lateral tire forces, F_{Yi} (Switching at t=15 seconds)

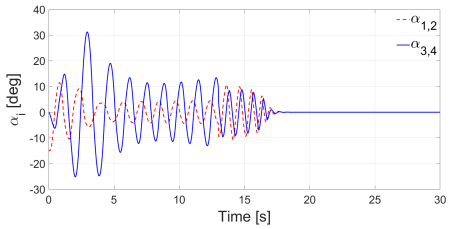

(c) Tire slip angles, α_i (Switching at t=13 seconds)

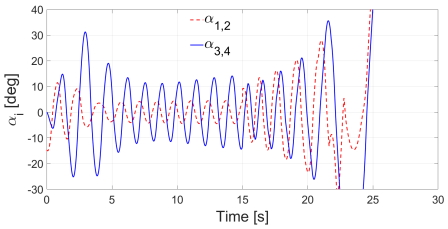

(d) Tire slip angles, α_i (Switching at t=15 seconds)

Figure 3.9: Evolution of lateral tire forces and tire slip angles for two different switching times: The exploited control allocation (CA) is switched from the fixed CA to a conventional optimal CA at t=13s in one case and at t=15s, in the other.

$t = 15s$.

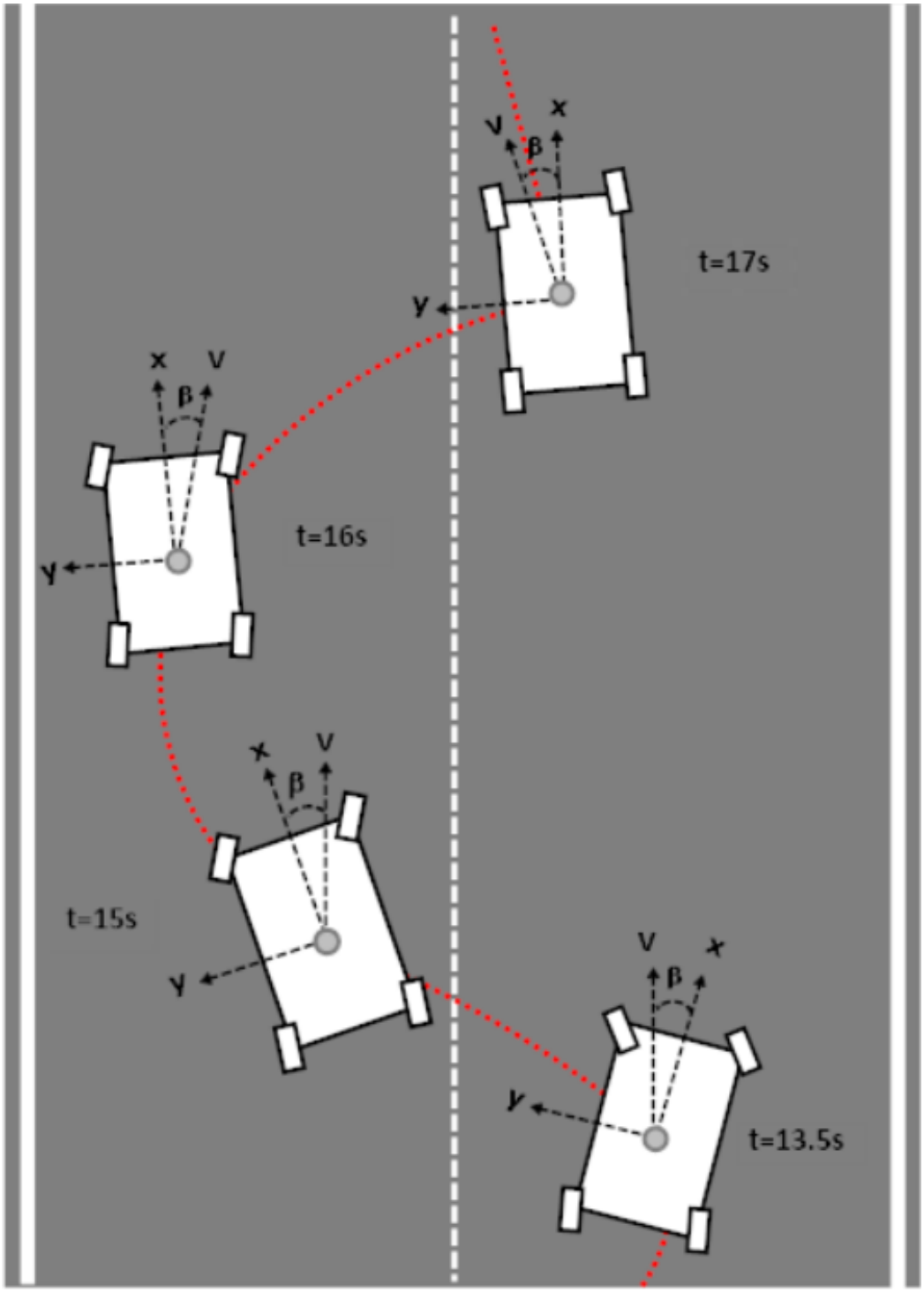

Figure 3.10: When the switch from the fixed control allocation (CA) to conventional CA occurs at t=13s, the conventional CA makes the tires align with the slip direction, which is the direction of the longitudinal velocity, V. This helps reduce side slip angle, β, and damps out the oscillations.

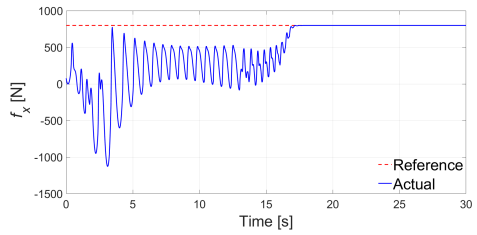

(a) Reference vs. actual longitudinal force (Switching at t=13s)

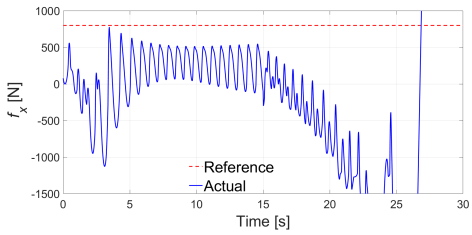

(b) Reference vs. actual longitudinal force (Switching at t=15s)

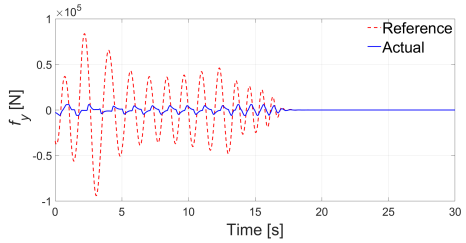

(c) Reference vs. actual lateral force (Switching at t=13s)

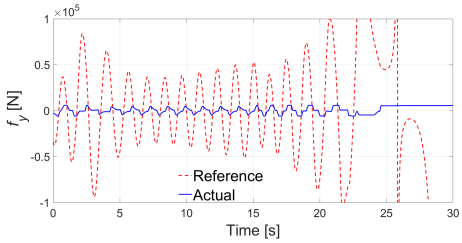

(d) Reference vs. actual lateral force (Switching at t=15s)

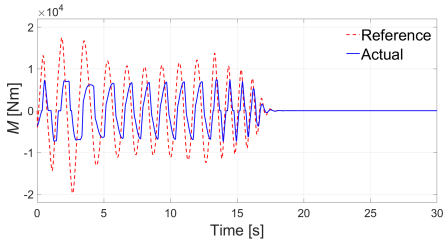

(e) Reference vs. actual yaw moment (Switching at t=13s)

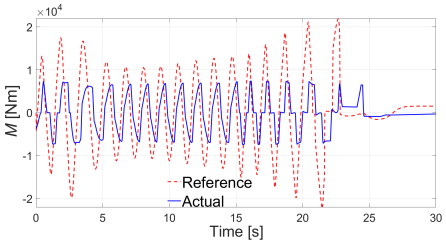

(f) Reference vs. actual yaw moment (Switching at t=15s)

Figure 3.11: Evolution of reference and actual forces and moments for two different switching times: The exploited control allocation (CA) is switched from the fixed CA to a conventional optimal CA at t=13s in one case and at t=15s, in the other.

3.3.3 Augmentation with Control Allocation for Recovering from Driver Induced Oscillations

In the second scenario, discussed in the previous subsection, we investigated two cases: in the first case, conventional optimal CA was activated at $t = 13s$ and in the second case at $t = 15s$. It was shown that in the later case, the vehicle could not recover stability. The scenario in this section is exactly the same as the later case until $t = 20s$. At $t = 20s$, we activate the proposed CA, described in

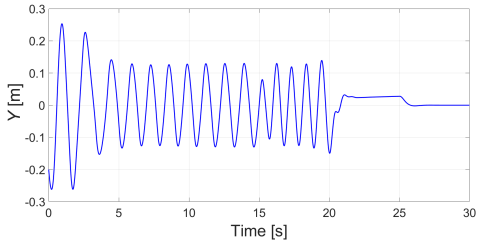

(a) Lateral displacement of the car center of gravity, Y.

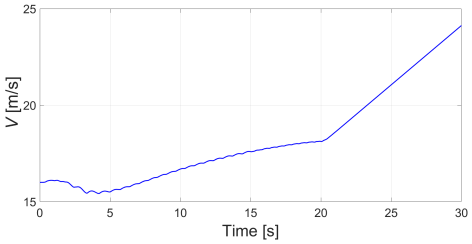

(b) Longitudinal velocity, V

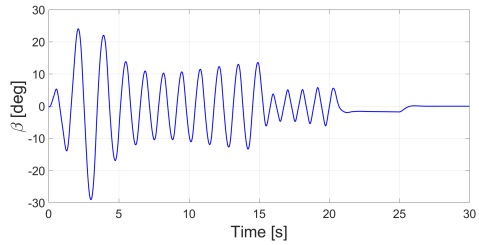

(c) Side slip angle, β

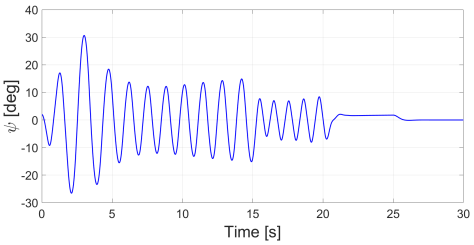

(d) Yaw angle, ψ

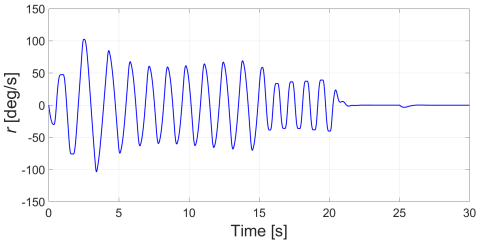

(e) Yaw rate, r

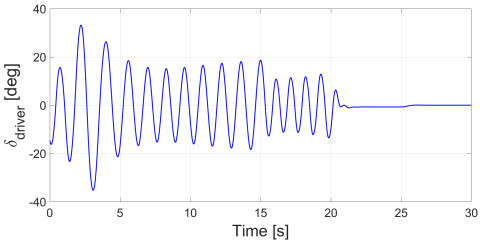

(f) Driver steering angle input, δ_{driver}

Figure 3.12: Evolution of system states and the driver steering input for the third scenario. The scenario starts with the fixed control allocation (CA), and at t=15s the conventional optimal CA is activated. Then, at t=20s the proposed CA is introduced and once the oscillations die out, the CA is switched back to the conventional optimal CA at t=25s.

Section 3.2.2. In other words, in the third and final scenario, the vehicle starts its motion with the initial conditions given in the beginning of Section 3.3, and with the fixed control allocator. Then, the conventional optimal CA is activated at $t = 15s$ and finally the proposed CA is activated at $t = 20s$. It is noted that the main difference between the conventional and the proposed CA is that while the former uses the cost function given in (3.25), the latter one uses the one given in (3.26), which contains an extra term that penalizes the difference between the derivatives of the reference and actual forces and moments. To make the effect of derivative difference term in (3.26) more pronounced, the weighting term Γ_d is

Table 3.1: Control allocation switching schedule in the third scenario.

$t = 0s - 15s$	$t = 15s - 20s$	$t = 20s - 25s$	$t = 25s$ onwards
Fixed CA	Conventional CA	Proposed CA	Conventional CA

selected as a very large number. Finally, after the oscillations are damped, the derivative error term is eliminated at $t = 25s$, which effectively makes the control allocator go back to its conventional CA form. The scenario is summarized in Table 3.1.

Fig. 3.12 shows the evolution of system states and the driver steering input for the final scenario. Shortly after the activation of the proposed CA at $t = 20s$, the oscillations die out. This is achieved by a careful manipulation of the CA outputs, which are shown in Fig. 3.13, via the minimization of the cost function (3.26). Related tire lateral forces and slip angles are provided in Fig. 3.14.

Fig. 3.15 demonstrates the time evolution of reference and actual forces and moments. It is important to notice that shortly after the proposed CA is activated at $t = 20$, the phase difference between the reference and actual signals are minimized, which eliminates the effective time delay introduction to the system and hence damps the oscillations. Phase difference minimization after the introduction of the proposed CA is shown more clearly at Fig. 3.15b and Fig. 3.15d, where zoomed versions of Fig. 3.15a and Fig. 3.15c for the time interval $t = 20s$ and $t = 25s$ are shown, respectively.

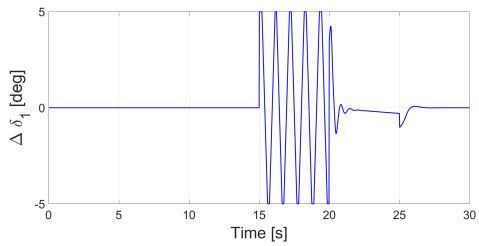

(a) Front steering correction angle, $\Delta\delta_1$

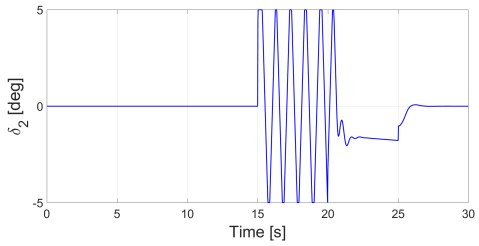

(b) Rear steering angle, δ_2

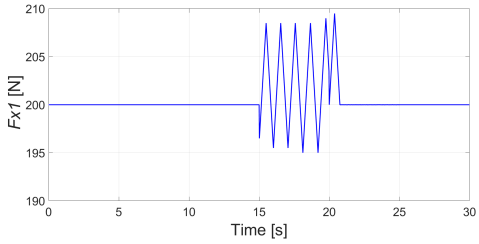

(c) Front left tire's longitudinal force, F_{X1}

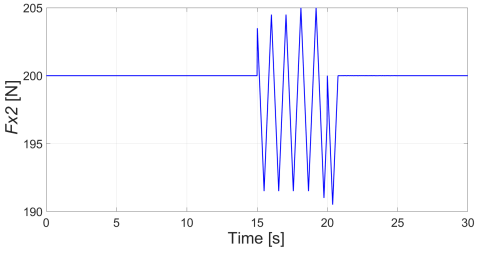

(d) Front right tire's longitudinal force, F_{X2}

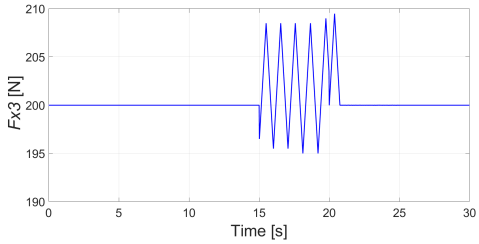

(e) Rear left tire's longitudinal force, F_{X3}

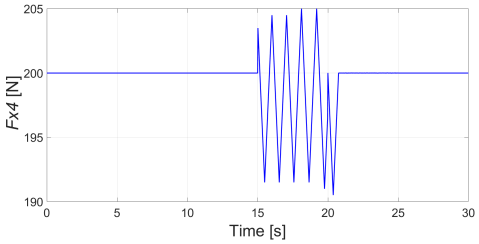

(f) Rear right tire's longitudinal force, F_{X4}

Figure 3.13: Evolution of CA outputs during the third scenario.

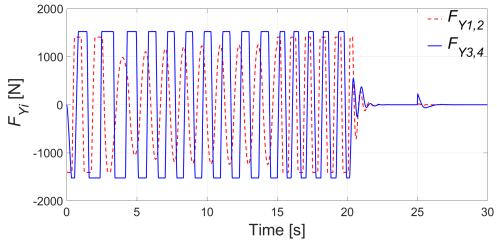

(a) Lateral tire forces, F_{Yi}

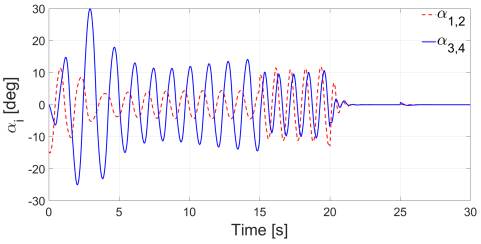

(b) Tire slip angles, α_i

Figure 3.14: Evolution of lateral tire forces and slip angles during the third scenario.

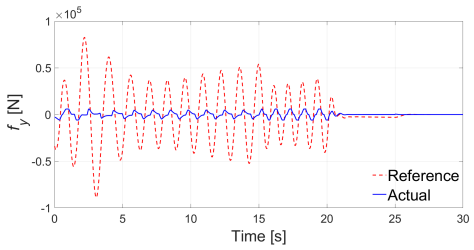

(a) Reference vs. actual lateral force

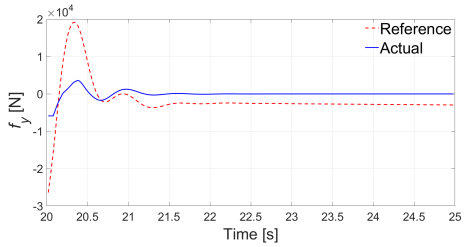

(b) Reference vs. actual lateral force (from t=20s to t=25s)

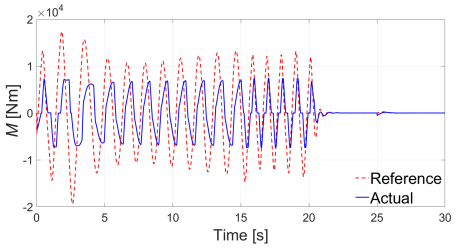

(c) Reference vs. actual yaw moment

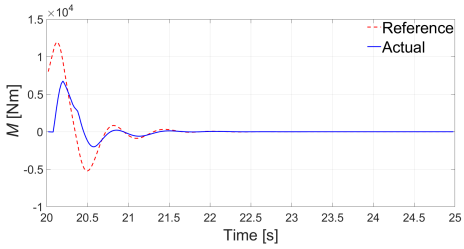

(d) Reference vs. actual yaw moment (from t=20s to t=25s)

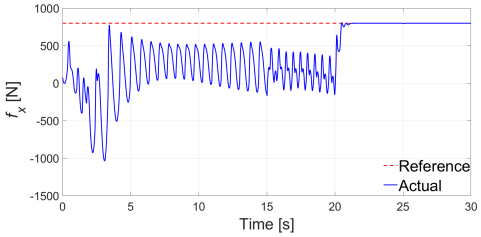

(e) Reference vs. actual longitudinal force

Figure 3.15: Evolution of reference and actual forces and moments during the third scenario.

Chapter 4

Handling Driver Induced Oscillations in the Presence of Actuator Effectiveness Uncertainty

In this chapter, an adaptive control allocation approach is exploited to recover from driver induced oscillations when effectiveness of the actuators are unknown. Actuator failures not only reduce the performance but can also lead to accidents. One way to address the actuator failure is using redundant actuators. Control allocation methodologies can be used for distributing the desired control effort among redundant actuators. The adaptive control allocation approach employed in this chapter to recover from driver induced oscillations is inspired from [34], where the main idea is to minimize the derivative error, instead of the error itself, between desired and achieved control efforts. Control allocation proposed in Chapter 3 is sufficient to make a vehicle get out of oscillations at high velocities on low friction road. However, in the presence of actuators failure, it may not be able to compensate the failure and the vehicle can become unstable. That is why, an adaptive version of the previously proposed control allocation approach is introduced in this chapter.

4.1 Problem Formulation and Solution

To model the actuator faults or loss of effectiveness, plant dynamics (3.10) can be re-written as

$$\dot{X} = AX + B_u \Upsilon u_n, \tag{4.1}$$

where $\Upsilon \in \mathcal{R}^{6\times6}$ is a diagonal matrix representing actuators uncertainty. As discussed in Section 3.2, since $B_u \in \mathcal{R}^{5\times6}$ is rank deficient, i.e. $rank(B_u) = 3 < 6$, it can be decomposed into two matrices as $B_u = B_v B$, where $B_v \in \mathcal{R}^{5\times3}$, and $B \in \mathcal{R}^{3\times6}$ has rank 3. Hence, (4.1) reduces to

$$\dot{X} = AX + B_v B \Upsilon u_n. \tag{4.2}$$

Decomposing u_n as $(u + \Delta u)$ to indicate the roles of the driver and the control allocator separately, (4.2) is rewritten as

$$\dot{X} = AX + B_v B \Upsilon (u + \Delta u). \tag{4.3}$$

The objective of the adaptive control allocation is to achieve $B\Upsilon(u + \Delta u) = v$, where v is the desired forces and moments, while minimizing the phase difference between these two signals. To achieve this goal, the control allocation problem is converted into a model reference adaptive control allocation problem. Consider the dynamics

$$\dot{y} = A_m y + B\Upsilon(\dot{u} + \dot{\Delta u}) - \dot{v}, \tag{4.4}$$

where $A_m \in \mathcal{R}^{3\times3}$ is a stable matrix, and a reference model

$$\dot{y}_m = A_m y_m. \tag{4.5}$$

The aim is to make the state vector, y in (4.4), converge to reference model output, y_m. Defining the derivative of the control input as

$$\dot{u} + \dot{\Delta u} = \Theta_v^T \dot{v}, \tag{4.6}$$

where $\Theta_v \in \mathcal{R}^{3\times6}$ is an adaptive parameter matrix which is to be determined, and substituting (4.6) in (4.4), we get

$$\dot{y} = A_m y + B\Upsilon\Theta_v^T \dot{v} - \dot{v},$$
$$\dot{y} = A_m y + (B\Upsilon\Theta_v^T - I)\dot{v}, \tag{4.7}$$

where $I \in \mathcal{R}^{3\times3}$ is an identity matrix. It is assumed that there exists an ideal solution for adaptive parameter, Θ_v^{*T} such that $B\Upsilon\Theta_v^{*T} = I$. Describing $\Theta_v^T = \Theta_v^{*T} + \tilde{\Theta}_v^T$, where $\tilde{\Theta}_v^T$ is the deviation of adaptive parameter Θ_v^T from its ideal value Θ_v^{*T}, (4.7) can be rewritten as

$$\dot{y} = A_m y + B\Upsilon\tilde{\Theta}_v^{\ T}\dot{v}. \tag{4.8}$$

Defining error dynamics as $e = y - y_m$ and subtracting (4.5) from (4.8), derivative of error can be written as

$$\dot{e} = A_m e + B\Upsilon\tilde{\Theta}_v^{\ T}\dot{v}. \tag{4.9}$$

Let $\Pi = \pi I \in \mathcal{R}^{3\times3}$ an adaptive gain matrix , where $\pi > 0$, is a positive scalar. Assuming that $\dot{v}$ is bounded, it can be shown [34] that the adaptive law

$$\dot{\Theta}_v = \Pi Proj(\Theta_v, -\dot{v}e^T PB) \tag{4.10}$$

results in a stable system with bounded signals, where $Proj$ is the projection operator [35], P is positive definite symmetric matrix solution of Lyapunov equation $A_m^T P + PA_m = -Q_{lyap}$, where Q_{lyap} is also a positive definite symmetric matrix.

This adaptive control allocation approach, whose structure is given in Fig. 4.1, inspired from [27], is used to determine control input, u, such that the error between $\dot{v}$ and $B\Upsilon(\dot{u} + \dot{\Delta}u)$ is minimized for a vehicle with actuator effectiveness uncertainty.

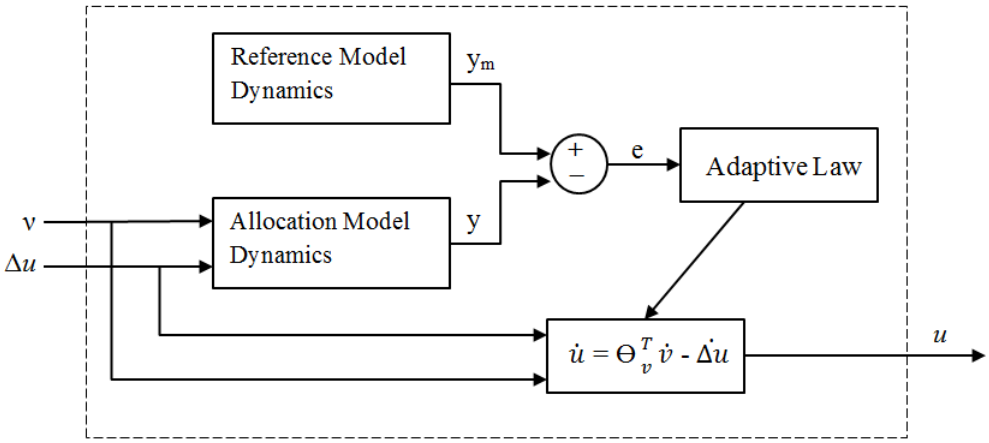

Figure 4.1: Block diagram of proposed adaptive CA.

4.2 Simulation Results

To demonstrate the effectiveness of the employed adaptive control allocation approach, a scenario is created within which the rear right tire bursts and loses 90% of its traction force. In the following two sub-sections, first, the scenario is explained in detail and a loss of stability is shown in the presence of fixed and conventional optimal control allocators. Secondly, the adaptive control allocation is introduced and the stability recovery is demonstrated. All the control allocation methods used in the simulations, except the adaptive one discussed above, are already explained in the previous chapters, and hence their working principles are omitted here.

4.2.1 Actuator Failure Scenario

The scenario starts with the fixed control allocation. At $t = 15s$, the conventional optimal control allocation is activated. At $t = 20s$ the "control allocation to recover from driver induced oscillations", proposed in Chapter 3 is activated and at the time of switching a 90% traction loss is introduced to the rear right tire to emulate a tire burst. The scenario is summarized in Table 4.1. It can be seen in Fig. 4.2 that under these scheduling conditions, the states grow unbounded after $t = 20s$. It can also be observed in Fig. 4.3 that at the time of switching to the "control allocation to recover from driver induced oscillations" at $t = 20s$, rear right tire's effectiveness is reduced to 10%. Both front and rear lateral forces are position saturated after $t = 20s$ (see Fig. 4.4). This control allocator is not designed for such a drastic failure and naturally can not stabilize the vehicle.

Table 4.1: Control allocation switching schedule with actuator failure.

$t = 0s - 15s$	$t = 15s - 20s$	$t = 20s$ onwards
Fixed CA	Conventional optimal CA	CA to recover from driver induced oscillations is introduced and rear right tire fails

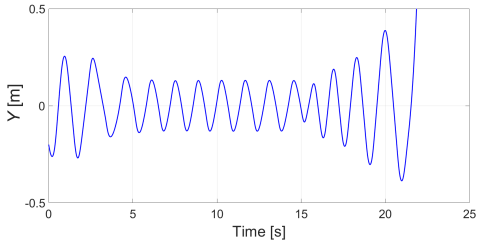

(a) Lateral displacement of the car center of gravity, Y.

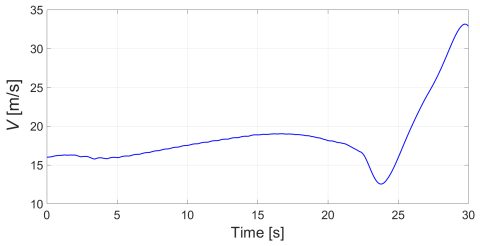

(b) Longitudinal velocity, V

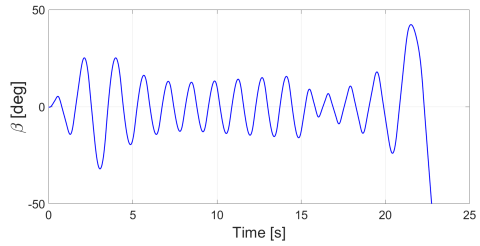

(c) Side slip angle, β

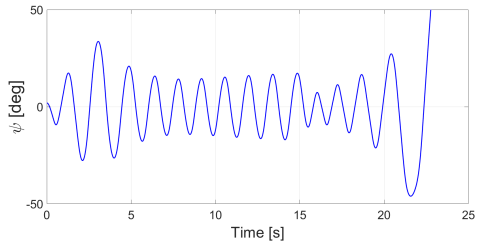

(d) Yaw angle, ψ

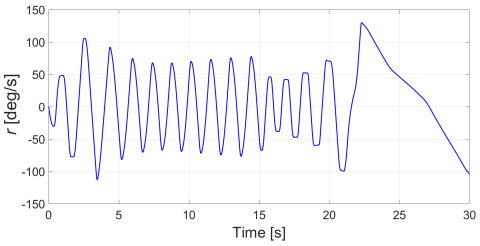

(e) Yaw rate, r

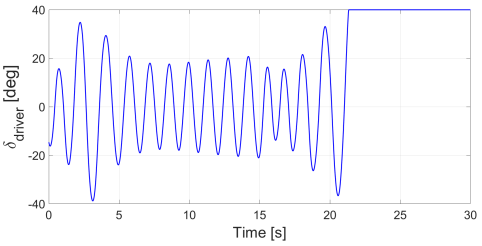

(f) Driver steering angle input, δ_{driver}

Figure 4.2: Evolution of system states and the driver steering input. The scenario starts with the fixed control allocation (CA), and at t=15s the conventional optimal CA is activated. Then, at t=20s the "control allocation to recover from driver induced oscillations", proposed in Chapter 3, is introduced and at the time of switching the rear right tire bursts and loses 90% of its traction.

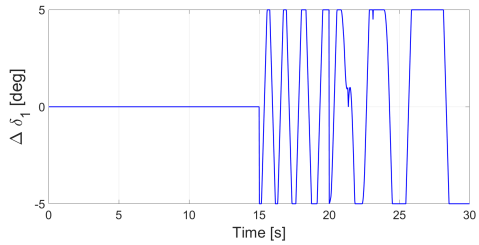

(a) Front steering correction angle, $\Delta\delta_1$

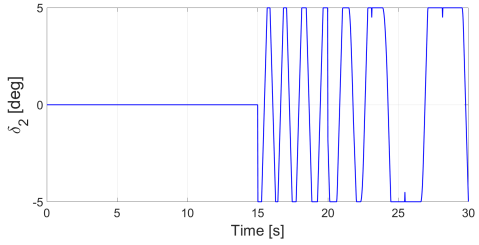

(b) Rear steering angle, δ_2

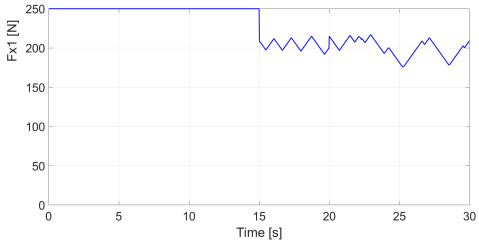

(c) Front left tire's longitudinal force, F_{X1}

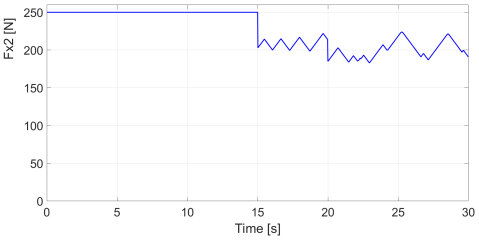

(d) Front right tire's longitudinal force, F_{X2}

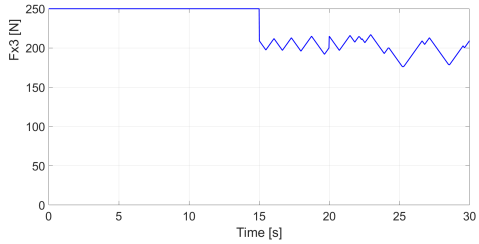

(e) Rear left tire's longitudinal force, F_{X3}

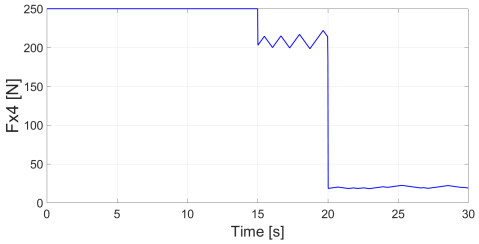

(f) Rear right tire's longitudinal force, F_{X4}

Figure 4.3: Evolution of CA outputs.

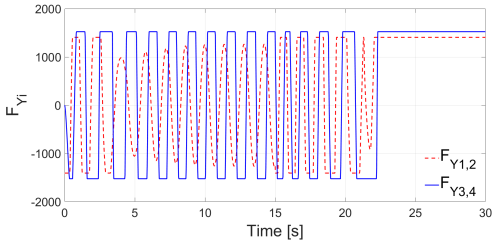

(a) Lateral tire forces, F_{Yi}

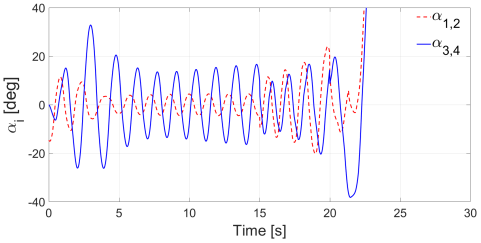

(b) Tire slip angles, α_i

Figure 4.4: Evolution of lateral tire forces and slip angles.

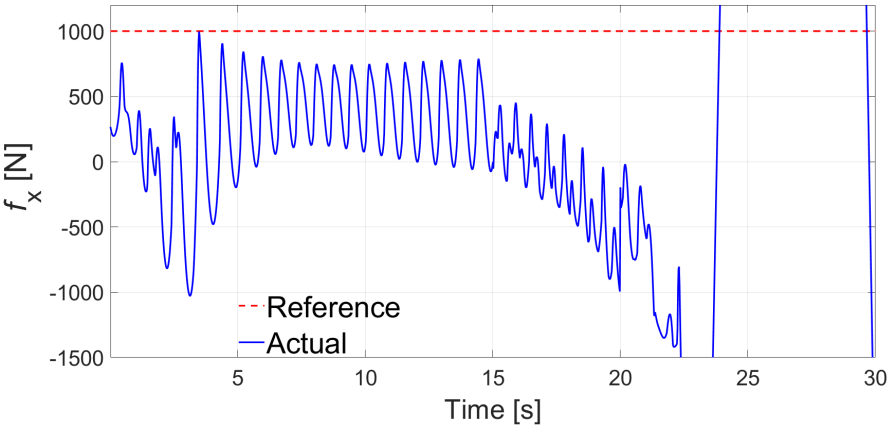

(a) Reference vs. actual longitudinal force

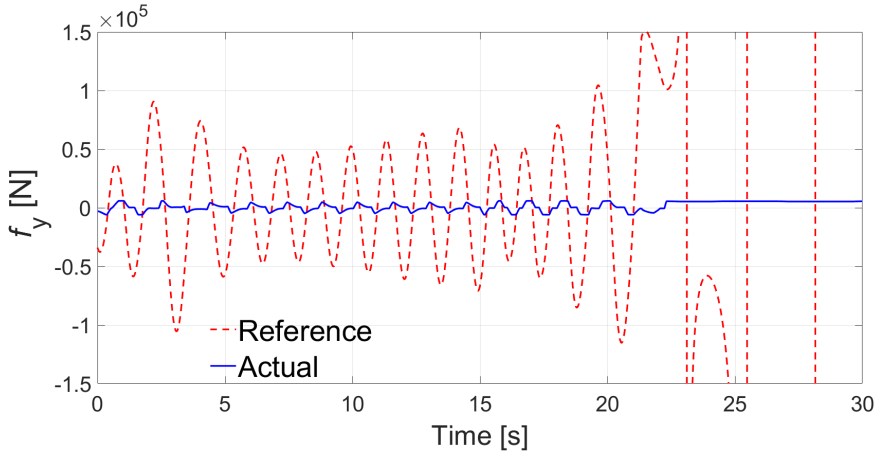

(b) Reference vs. actual lateral force

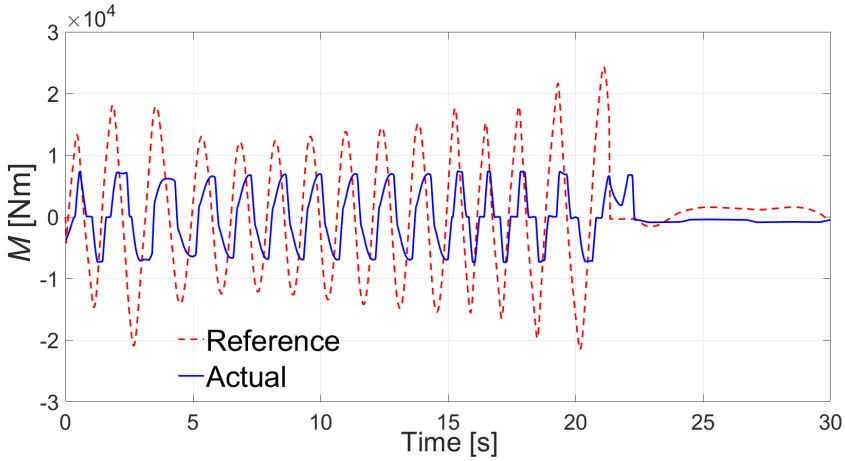

(c) Reference vs. actual yaw moment

Figure 4.5: Evolution of reference and actual forces and moments.

4.2.2 Adaptive Control Allocation Introduction

The same scenario as in the previous Section 4.2.1 is used. The only difference here is that at $t = 21s$ the adaptive control allocation is introduced. The scenario is summarized in Table 4.2. The adaptive control allocation is able to stop the oscillations from growing (see states in Fig. 4.6). It can be seen in Fig. 4.7 that once activated, the adaptive control allocation reduces the traction forces of the healthy tires as well in order to reduce the vehicle velocity so that the tires can get back the lateral and longitudinal grip on the road. Eventually, lateral tire forces and slips decrease which help the tires get back their grip on the road (see Fig. 4.8).

Table 4.2: Control allocation switching schedule with proposed adaptive CA.

$t = 0s - 15s$	$t = 15s - 20s$	$t = 20s - 21s$	$t = 21s$ onwards
Fixed CA	Conventional optimal CA	CA to recover from driver induced oscillations is introduced and rear right tire fails	Adaptive CA

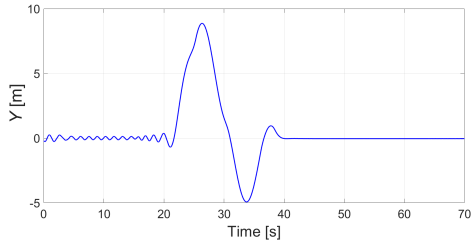

(a) Lateral displacement of the car center of gravity, Y.

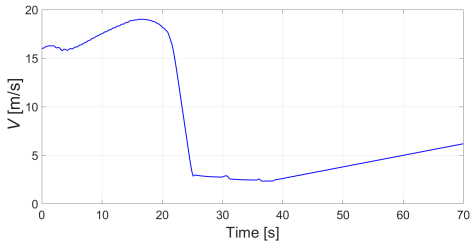

(b) Longitudinal velocity, V

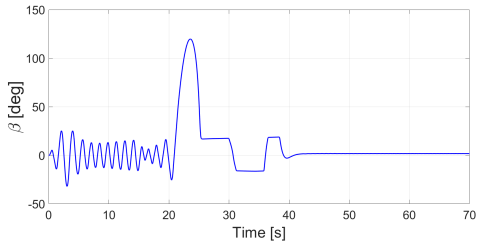

(c) Side slip angle, β

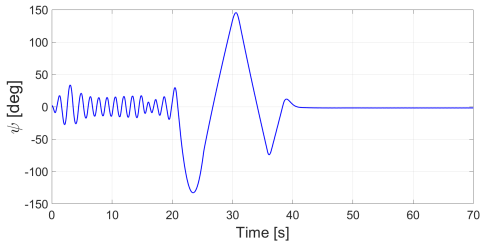

(d) Yaw angle, ψ

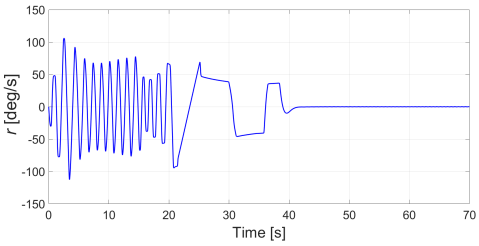

(e) Yaw rate, r

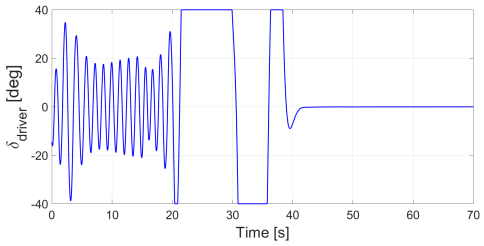

(f) Driver steering angle input, δ_{driver}

Figure 4.6: Evolution of system states and the driver steering input. The scenario starts with the fixed control allocation (CA). At t=15s the conventional optimal CA is activated and at t=20s the CA to recover from driver induced oscillations is activated and at the time of switching rear right tire fails. Then, at t=21s the adaptive CA is introduced.

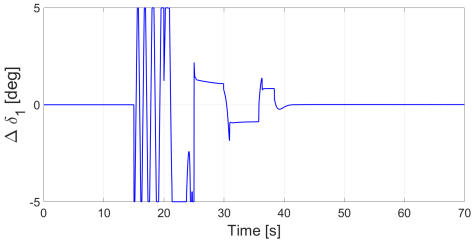

(a) Front steering correction angle, $\Delta\delta_1$

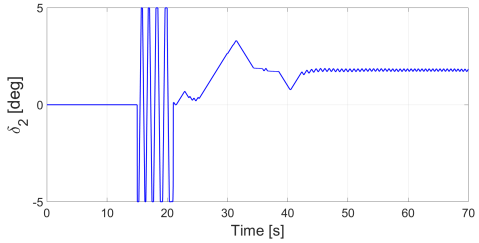

(b) Rear steering angle, δ_2

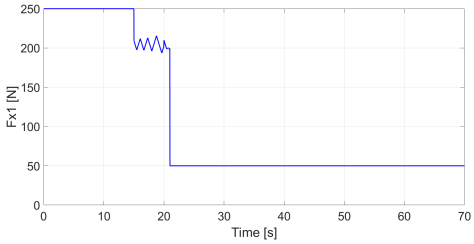

(c) Front left tire's longitudinal force, F_{X1}

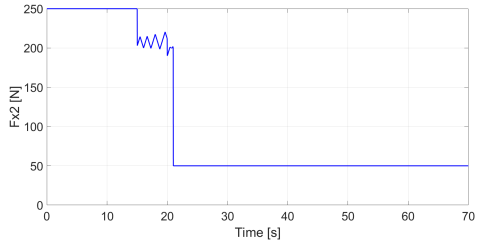

(d) Front right tire's longitudinal force, F_{X2}

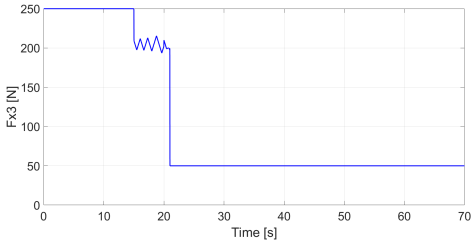

(e) Rear left tire's longitudinal force, F_{X3}

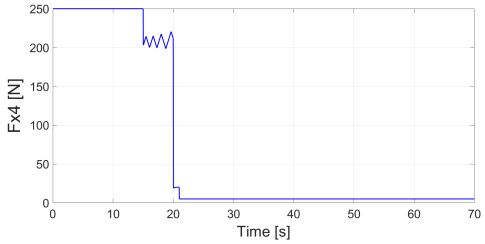

(f) Rear right tire's longitudinal force, F_{X4}

Figure 4.7: Evolution of CA outputs.

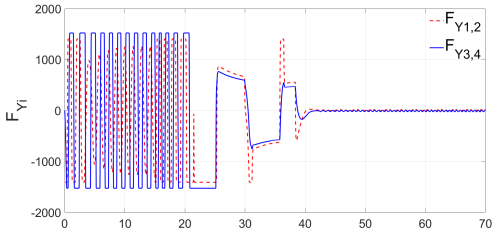

(a) Lateral tire forces, F_{Yi}

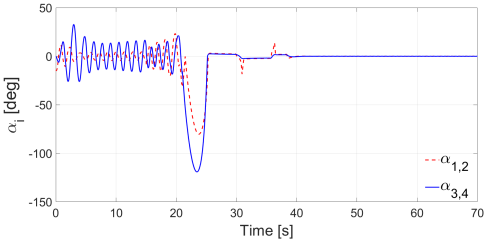

(b) Tire slip angles, α_i

Figure 4.8: Evolution of lateral tire forces and slip angles.

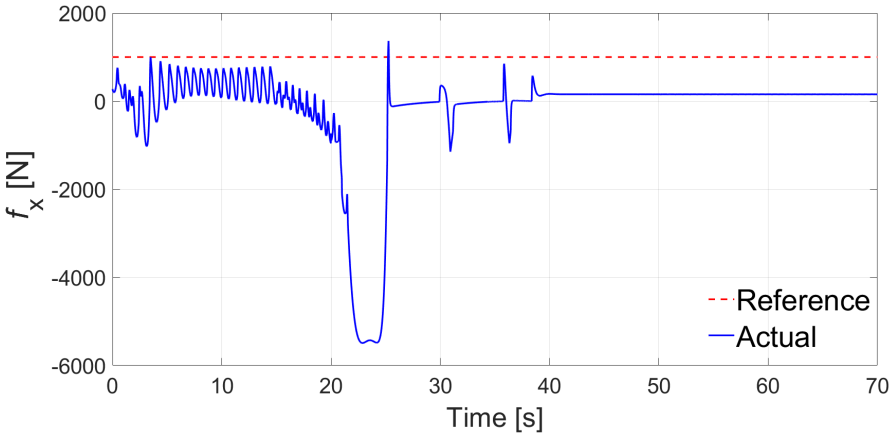

(a) Reference vs. actual longitudinal force

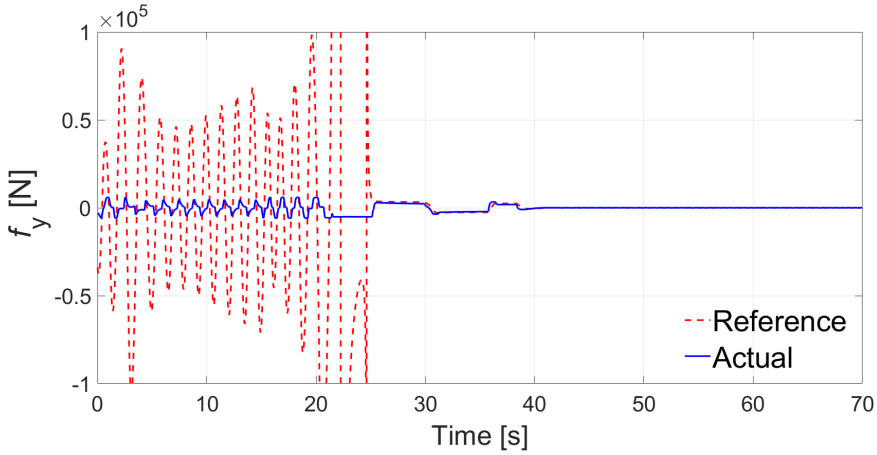

(b) Reference vs. actual lateral force

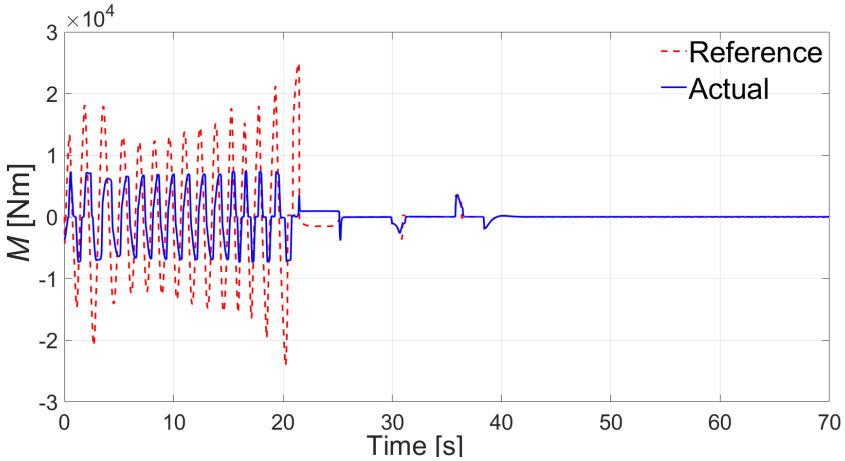

(c) Reference vs. actual yaw moment

Figure 4.9: Evolution of reference and actual forces and moments.

Chapter 5

Conclusion and Future Work

A comprehensive study about fishtailing is rarely, if at all, found in the open literature. In this thesis, a conceptual background of fishtailing motion is investigated with the help of accompanying mathematical equations. Using a specific vehicle configuration, where vehicle center of gravity is close to the rear end, fishtailing motion is created under low friction and high velocity conditions. It is observed that the rear end of the car being heavier than the front causes more centrifugal force effect at the rear, which gives rise to more deflection at rear tire-road contact patch resulting in higher slip angles at the rear tires. The increase in tire slip angle, α, increases cornering force in general but this is true up to a certain threshold value ($\approx 5^o$). After this value, the tire hits its lateral force saturation limit and starts skidding. Rear tires having more cornering stiffness due to more normal load compared to the front tires, is another reason for the rear tires being more prone to reaching the lateral force saturation limits. Combined with driver's over-compensating corrective actions, rear tire slippage instigates the fishtailing motion.

It is observed through simulations that conventional optimal control allocation approaches based on error minimization between reference, v, and actual forces/-moments, $B(u + \Delta u)$, are sufficient to make the vehicle get out of an oscillatory

motion, at low velocities. However, at high velocities, conventional optimal control allocation methods fail to damp the oscillations. Hence, a control allocation approach based on derivative error minimization between v and $B(u + \Delta u)$ is presented in this thesis that can minimize the effective time delay between driver intended signals and vehicle's responses, which eventually makes the vehicle get out of oscillatory fishtailing motion.

An adaptive version of the investigated control allocation method is also tailored for driver induced oscillation recovery. An actuator failure scenario is investigated to demonstrate the capabilities of this adaptive control allocator. In this scenario, one of the tires loses its pressure resulting in a 90% effectiveness loss. Such a failure not only degrades the performance of the vehicle but can also cause an accident. It is shown in the simulation studies that the adaptive version of the control allocator is capable of recovering vehicle stability in cases where the other alternatives fail.

For future work, different actuator failure scenarios can be investigated to observe the limitations of the control allocation methods studied in this thesis. These limitations may induce further theoretical developments.

Bibliography

[1] G. Jeram and J. Prasad, "Tactile avoidance cueing for pilot induced oscillation," in *AIAA Atmospheric Flight Mechanics Conference and Exhibit*, p. 5311, 2003.

[2] D. T. McRuer, "Pilot-induced oscillations and human dynamic behavior," 1995.

[3] K. C. C. David H. Weir, "Review of control theory models for directional and speed control," in *Modelling driver behaviour in automotive environments: critical issues in driver interactions with intelligent transport systems* (P. C. Cacciabue, ed.), ch. 17, Springer, 2007.

[4] H. F. Grip, L. Imsland, T. A. Johansen, J. C. Kalkkuhl, and A. Suissa, "Vehicle sideslip estimation," *IEEE control systems magazine*, vol. 29, no. 5, pp. 36–52, 2009.

[5] M. C. A. Galip Ulsoy, Huei Peng, *Automotive control systems*. New York: Cambridge university press, 2012.

[6] R. Rajamani, *Vehicle dynamics and control*. New York: Springer, 2005.

[7] K. Nam, S. Oh, H. Fujimoto, and Y. Hori, "Robust yaw stability control for electric vehicles based on active front steering control through a steer-by-wire system," *International Journal of Automotive Technology*, vol. 13, no. 7, pp. 1169–1176, 2012.

[8] H. E. Russell and J. C. Gerdes, "Design of variable vehicle handling characteristics using four-wheel steer-by-wire," *IEEE Transactions on Control Systems Technology*, vol. 24, no. 5, pp. 1529–1540, 2016.

[9] J. Lee, J. Choi, K. Yi, M. Shin, and B. Ko, "Lane-keeping assistance control algorithm using differential braking to prevent unintended lane departures," *Control Engineering Practice*, vol. 23, pp. 1–13, 2014.

[10] M. Croft-White and M. Harrison, "Study of torque vectoring for all-wheel-drive vehicles," *Vehicle system dynamics*, vol. 44, no. sup1, pp. 313–320, 2006.

[11] M. B. Alberding, J. Tjønnås, and T. A. Johansen, "Integration of vehicle yaw stabilisation and rollover prevention through nonlinear hierarchical control allocation," *Vehicle system dynamics*, vol. 52, no. 12, pp. 1607–1621, 2014.

[12] E. Joa, K. Yi, K. Sohn, and H. Bae, "Four-wheel independent brake control to limit tire slip under unknown road conditions," *Control Engineering Practice*, vol. 76, pp. 79–95, 2018.

[13] Q. Tan, X. Wang, J. Taghia, and J. Katupitiya, "Force control of two-wheel-steer four-wheel-drive vehicles using model predictive control and sequential quadratic programming for improved path tracking," *International Journal of Advanced Robotic Systems*, vol. 14, no. 6, p. 1729881417746295, 2017.

[14] F. Wang and Y. Chen, "Dynamics and control of a novel active yaw stabilizer to enhance vehicle lateral motion stability," *Journal of Dynamic Systems, Measurement, and Control*, vol. 140, no. 8, p. 081007, 2018.

[15] Z. Shuai, H. Zhang, J. Wang, J. Li, and M. Ouyang, "Lateral motion control for four-wheel-independent-drive electric vehicles using optimal torque allocation and dynamic message priority scheduling," *Control Engineering Practice*, vol. 24, pp. 55–66, 2014.

[16] S. Di Cairano, H. E. Tseng, D. Bernardini, and A. Bemporad, "Vehicle yaw stability control by coordinated active front steering and differential braking in the tire sideslip angles domain," *IEEE Transactions on Control Systems Technology*, vol. 21, no. 4, pp. 1236–1248, 2013.

[17] H. Zhou, F. Jia, H. Jing, Z. Liu, and L. Güvenç, "Coordinated longitudinal and lateral motion control for four wheel independent motor-drive electric vehicle," *IEEE transactions on Vehicular Technology*, vol. 67, no. 5, pp. 3782–3790, 2018.

[18] D. Kasinathan, A. Kasaiezadeh, A. Wong, A. Khajepour, S.-K. Chen, and B. Litkouhi, "An optimal torque vectoring control for vehicle applications via real-time constraints," *IEEE Transactions on Vehicular Technology*, vol. 65, no. 6, pp. 4368–4378, 2016.

[19] R. Attia, R. Orjuela, and M. Basset, "Dual-mode control allocation for integrated chassis stabilization," *IFAC Proceedings Volumes*, vol. 47, no. 3, pp. 11219–11224, 2014.

[20] J. Ni, J. Hu, and C. Xiang, "Envelope control for four-wheel independently actuated autonomous ground vehicle through afs/dyc integrated control," *IEEE Transactions on Vehicular Technology*, vol. 66, no. 11, pp. 9712–9726, 2017.

[21] J. Tjønnås and T. A. Johansen, "Stabilization of automotive vehicles using active steering and adaptive brake control allocation," *IEEE Transactions on Control Systems Technology*, vol. 18, no. 3, pp. 545–558, 2010.

[22] G. Park and S. B. Choi, "Optimal brake distribution for electronic stability control using weighted least square allocation method," in *2016 16th International Conference on Control, Automation and Systems (ICCAS)*, pp. 1420–1425, IEEE, 2016.

[23] A. Tavasoli, M. Naraghi, and H. Shakeri, "Optimized coordination of brakes and active steering for a 4ws passenger car," *ISA transactions*, vol. 51, no. 5, pp. 573–583, 2012.

[24] J. Zhao, P. K. Wong, X. Ma, and Z. Xie, "Chassis integrated control for active suspension, active front steering and direct yaw moment systems using hierarchical strategy," *Vehicle System Dynamics*, vol. 55, no. 1, pp. 72–103, 2017.

[25] J. Wang and R. G. Longoria, "Coordinated vehicle dynamics control with control distribution," in *2006 American control conference*, pp. 6–pp, IEEE, 2006.

[26] X. Yang, Z. Wang, and W. Peng, "Coordinated control of afs and dyc for vehicle handling and stability based on optimal guaranteed cost theory," *Vehicle System Dynamics*, vol. 47, no. 1, pp. 57–79, 2009.

[27] O. Temiz, M. Çakmakcı, and Y. Yildiz, "A fault tolerant vehicle stability control using adaptive control allocation," in *ASME 2018 Dynamic Systems and Control Conference*, pp. V001T09A002–V001T09A002, American Society of Mechanical Engineers, 2018.

[28] D. M. Acosta, Y. Yildiz, R. W. Craun, S. D. Beard, M. W. Leonard, G. H. Hardy, and M. Weinstein, "Piloted evaluation of a control allocation technique to recover from pilot-induced oscillations," *Journal of Aircraft*, vol. 52, no. 1, pp. 130–140, 2014.

[29] Y. Yildiz and I. Kolmanovsky, "Stability properties and cross-coupling performance of the control allocation scheme capio," *Journal of Guidance, Control, and Dynamics*, vol. 34, no. 4, pp. 1190–1196, 2011.

[30] H. Pacejka, *Tire and vehicle dynamics*. Elsevier, 2005.

[31] M. Aripin, Y. Md Sam, K. A. Danapalasingam, K. Peng, N. Hamzah, and M. Ismail, "A review of active yaw control system for vehicle handling and stability enhancement," *International journal of vehicular technology*, vol. 2014, 2014.

[32] D. Klyde and D. Mitchell, "A pio case study-lessons learned through analysis," in *AIAA Atmospheric Flight Mechanics Conference and Exhibit*, p. 5813, 2005.

[33] A. Tuononen, T. Lehtonen, and M. Juhala, "Estimation of tyre cornering stiffness from vehicle measurements," in *FISITA 2006 World Automotive Congress*, 2006.

[34] S. S. Tohidi, Y. Yildiz, and I. Kolmanovsky, "Pilot induced oscillation mitigation for unmanned aircraft systems: An adaptive control allocation approach," in *2018 IEEE Conference on Control Technology and Applications (CCTA)*, pp. 343–348, IEEE, 2018.

[35] E. Lavretsky and T. E. Gibson, "Projection operator in adaptive systems," *arXiv preprint arXiv:1112.4232*, 2011.